sustainability

MDPI

Article

Effects of Thermal Power Flexibility Retrofits on Renewable Energy Integration in China's Power System: An 8760-Hour Assessment of Curtailment and Unserved Energy

Rong Li [1], Changchun Zhou [1], Chenlin Song [2], Cheng Zhong [2], Tiantian Feng [2,3,4] and Xianyue Shen [2,*]

[1] Global Energy Interconnection Group Co., Ltd., Xicheng District, Beijing 100031, China; rong-li@geidco.org (R.L.); changchun-zhou@geidco.org (C.Z.)
[2] School of Economics and Management, China University of Geosciences (Beijing), Beijing 100083, China; 17280320869@163.com (C.S.); cheng4754105@163.com (C.Z.); fengtiantian89@163.com (T.F.)
[3] MOE Social Science Laboratory of Mineral Resources Security Governance, China University of Geosciences (Beijing), Beijing 100083, China
[4] Hainan Institute, China University of Geosciences (Beijing), Sanya 572000, China
* Correspondence: shenxianyue0224@163.com; Tel.: +86-13121908577

Abstract

Integrating growing wind and solar generation while maintaining supply adequacy is a key challenge for sustainable power systems. However, the effects of different thermal retrofit pathways on renewable curtailment and modeled unserved energy remain unclear as renewable capacity expands. This study compares deep peak-shaving, fast-ramping, and combined retrofits using a PyPSA baseline and an 8760-h system dynamics simulation covering 31 Chinese provincial nodes. Doubling renewable capacity increases actual wind and solar generation by 51.4%, while the utilization rate falls from 91.4% to 69.2%. At baseline renewable capacity, the deep peak-shaving scenario S1 reduces annual curtailment by 25.0 TWh but produces 45.49 GWh of modeled unserved energy. S1 also reduces curtailment at renewable capacity multipliers of 1.50 and 2.00, whereas the fast-ramping scenario S2 has little effect on annual curtailment. At equal 50% retrofit coverage, the combined scenario S3 preserves S1's curtailment benefit while nearly eliminating its supply shortfall. The expanded combined scenario S4, with 80% coverage, further reduces curtailment to 234.9 TWh at baseline renewable capacity. Considering curtailment and modeled unserved energy jointly, the combined retrofit provides the most favorable outcome among the equal-coverage pathways for supporting renewable integration while maintaining supply adequacy.

Keywords: thermal flexibility; renewable integration; renewable curtailment; deep turndown; ramping; unserved energy

Academic Editor: Grigorios L. Kyriakopoulos

Received: 15 September 2026
Revised: 23 October 2026
Accepted: 30 October 2026
Published: 31 October 2026

Copyright: © 2026 by the authors. Licensee MDPI, Basel, Switzerland. This article is an open access article distributed under the terms and conditions of the Creative Commons Attribution (CC BY) license.

1. Introduction

By the end of 2025, China's cumulative grid-connected wind and solar capacity reached 1.84 TW, accounting for 47% of total installed generation capacity [1]. China's power-system flexibility plan for 2025–2027 aims to accommodate annual additions of more than 200 GW of renewable capacity and achieve a national renewable utilization rate of at least 90% by 2027 [2]. As wind and solar deployment increases, weather-driven output does not always coincide with hourly electricity demand [3]. Operational priorities

are therefore shifting from annual energy adequacy to hourly power balancing. Steep net-load ramps can occur when renewable output falls or demand rises [3]. Continuous hourly simulation is needed to identify the timing and mechanisms of supply–demand mismatches. For sustainable power-system operation, renewable electricity must be used more effectively without compromising hourly supply adequacy.

Research quantifying the effects of thermal power flexibility retrofits on renewable energy integration has evolved beyond comparisons of individual technical parameters. Retrofits are increasingly assessed alongside dispatch strategies and market mechanisms. Ye et al. assessed thermal power unit flexibility requirements under future renewable energy scenarios in China. They found that lower minimum load levels can reduce curtailment, although the benefits depend on the renewable deployment pathway [4]. A planning study for Yunnan incorporated coal-fired power flexibility retrofits and battery storage into a capacity-expansion and dispatch model. The effects of retrofits on curtailment, coal-fired generation, and system costs were quantified [5]. Another study combined mixed-integer linear programming with unit commitment modeling to evaluate thermal power flexibility retrofits and a deep peak regulation ancillary service market. Retrofit benefits were found to depend on market rules and operating strategies [6]. Related studies of marginal curtailment examined how the integration value of additional renewable generation varies with system conditions [7,8]. Other studies investigated coordination between storage and thermal power deep peak regulation [9], and flexible capacity requirements in China [10]. Portfolios of flexibility resources were also examined in other power system [11,12]. These studies demonstrate the importance of retrofits, storage, and other flexibility resources for renewable integration. However, most focus on specific planning objectives or resource portfolios. A unified hourly comparison of minimum stable output, downward ramping, and upward ramping constraints during continuous operation remains limited. In particular, the timing of each binding constraint and shifts in the dominant constraint require further investigation.

Full-year chronological simulation provides the temporal resolution needed to identify these constraints. Studies of China's power system have used chronological operation or 8760-h production simulation. These studies examined temporal coordination among peak regulation ancillary services, wind and solar output, pumped storage, and thermal units [13,14]. Inter-provincial interconnection and reserve requirements in China's high-renewable power system have also been assessed. The analysis used multiple years of hourly wind and solar output and demand data [15]. Optimization frameworks such as PyPSA can represent multi-period operation and constraints on renewable generation, storage, and conventional generating units [16]. A multi-energy planning study of China combined capacity planning with hourly operational analysis to compare investment and operating outcomes [17]. These studies provide important foundations for chronological simulation and optimization modeling. Optimization models primarily identify optimal dispatch or capacity configuration under specified objectives and constraints. Further scenario analysis is needed to determine when individual thermal power constraints become binding. The effects of shifts between constraints on curtailment and supply shortfalls also need to be clarified. The limits of retrofit effectiveness at different renewable capacity levels require further examination.

Accordingly, three related questions are addressed in this study. First, how does renewable capacity expansion affect hourly profiles of available renewable output and net load over a full year? Second, when do minimum stable output, downward ramping, and upward ramping constrain system balancing, and how do their effects differ across scenarios? Third, how do alternative retrofit pathways affect curtailment and modeled supply shortfalls at higher renewable capacity levels? Continuous 8760-h scenario simulations are conducted using baseline operating time series from PyPSA. Actual renewable

generation, curtailment, utilization rates, and modeled supply shortfalls are compared across retrofit pathways. The hourly distribution of each outcome is also examined. The analysis focuses on when constraints become binding and how their effects propagate through system operation. The aim is to complement optimization studies of optimal dispatch and capacity configuration. Different retrofit pathways are compared in terms of their operational mechanisms, effects, and conditions of applicability.

2. Literature Review

2.1. Renewable Energy Variability and Power System Flexibility Requirements

As wind and solar penetration increases, power systems must balance changes in net load, defined as demand minus renewable output. Renewable output is influenced by weather and exhibits variability, uncertainty, and temporal mismatches with demand. These characteristics may deepen net load troughs, widen peak-to-valley differences, and increase hourly and sub-hourly regulation requirements [18,19]. Flexibility requirements must therefore be assessed in terms of adjustment magnitude, response speed, duration, and forecast uncertainty.

High solar output around midday can depress net load. In the evening, declining solar output may coincide with rising demand, creating substantial upward ramping requirements [20,21]. High renewable penetration also increases net load variability and forecast uncertainty, leading to more frequent short-term ramping requirement. Flexible ramping products have therefore been introduced in electricity markets, including those in the United States. Upward and downward ramping capacity is reserved to manage imbalances caused by rapid changes in renewable output [22]. Using Chinese power system data, Hou et al. showed that high solar penetration increases uncertainty in net load troughs and ramping requirements. Conventional representative-day profiles may therefore fail to capture the occurrence probabilities of different operating conditions [23]. Accordingly, both downward regulation during low net load periods and upward regulation following renewable output declines must be considered.

Flexibility requirements are commonly quantified using net load change rates, ramp magnitudes, event durations, and occurrence frequencies [24]. Forecast uncertainty has also been incorporated into assessments of ramping reserve requirements. Li et al. used probabilistic solar forecasts to estimate ramping requirements dynamically. Their results showed that reserve allocation based solely on historical net load changes may be insufficient or excessive. Incorporating updated forecast uncertainty can improve estimates of the required ramping capability [25]. Comparison of wind, solar, load, and net load ramping events reveal different patterns, even at relatively low renewable penetration. As penetration increases, net load ramping events can become frequent and temporally complex [26,27].

These studies hay broadened the geographical coverage of flexibility assessments and extended deterministic analyses to include forecast uncertainty. Assessment metrics have also expanded beyond peak-to-valley differences to capture ramp magnitude, duration, frequency, and reserve requirements. However, much of this literature focuses on the amount of flexibility required. Further analysis is needed to determine when these requirements exceed specific thermal power operating limits. The resulting interactions and shifts in binding constraints during continuous operation also warrant examination.

2.2. Thermal Power Flexibility and Renewable Integration

Rising net load ramps require closer matching between system flexibility requirements and available regulating resources [26]. Under the current generation mix, thermal

power remains important for peak regulation, reserves, and electricity supply. Its flexibility depends on minimum stable output, the feasible operating range, and ramping capability. González-Salazar et al. compared the technical flexibility of coal- and gas-fired power plants. Minimum load, ramp rates, start-up and shutdown processes, and minimum downtime were examined. The review showed that flexibility differs across plant types and cannot be adequately represented by a single peak regulation indicator [28]. Gas-fired units often provide faster ramping and start-up responses, although performance depends on plant technology and operating conditions. The dynamic response of coal-fired units is additionally constrained by thermal inertia.

System-level studies have also examined the economic and dispatch implications of flexible thermal operation. The National Renewable Energy Laboratory assessed the additional costs of cycling and wear associated with low-load operation, frequent starts and stops, and ramping. In the analyzed scenarios, these additional costs were outweighed by production cost savings from renewable generation displacing fossil fuel use [29]. Minimum output and ramp rates were also identified as important influences on curtailment. Their effects varied with solar penetration, indicating that the benefits of thermal flexibility depend on system conditions [30]. Regional production simulations have further incorporated minimum output, minimum up and down times, ramp rates, and start-up costs into high-renewable scenarios [31].

Minimum stable output determines how far thermal generation can be reduced during low net load periods. Research on net load forecasting under high solar penetration has emphasized the importance of identifying peaks and troughs [32]. When renewable output is concentrated in low-demand periods, a high minimum output can restrict further reductions in thermal generation. Lowering this limit through deep peak regulation can create additional room for renewable energy integration. However, this additional operating range can be fully used only if the required output adjustments satisfy other operating constraints. Lower minimum output alone therefore does not guarantee that all available renewable generation can be accommodated.

Ramping capability determines whether thermal power units can follow net load changes within the required time interval [33]. Multi-timescale planning studies have jointly considered thermal power retrofits and storage when assessing upward and downward flexibility [34]. Insufficient downward ramping can prevent timely reductions in thermal output as renewable generation increases, thereby causing curtailment. Insufficient upward ramping can limit supply responses when renewable output falls or demand rises, potentially affecting supply reliability [35]. Upward and downward ramping performance can differ with thermal processes, control strategies, and operating conditions. Recent unit commitment studies have therefore modeled the two directions separately to represent output adjustments across consecutive periods more accurately [36].

The literature has progressed from comparisons of plant-level technical performance to system-level analyses of dispatch costs and flexibility provision. The international studies reviewed here emphasize minimum load, ramping, start-up performance, cycling costs, and emissions. Studies of China have placed greater emphasis on deep peak regulation, ancillary services, and renewable energy integration. Together, these approaches clarify both the technical capabilities of thermal units and their economic consequences. Further comparison is needed to trace when the three constraints dominate and whether relieving one shifts the bottleneck to another.

2.3. Hourly-Scale Power System Simulation and System Dynamics Applications

Annual, monthly, and representative-day analyses may omit important chronological changes in wind and solar output and demand. Full-year hourly simulation preserves

these changes and enables operating constraints to be evaluated across consecutive periods. Existing studies have represented unit operating ranges, ramp rates, and storage operation within chronological frameworks to assess curtailment and flexibility requirements [13]. Planning models with 8760-h resolution have also been developed to capture seasonal and hourly variations in demand and renewable output [37]. Chronological production studies further indicate that monthly or representative-day approaches may overlook short but consequential curtailment and supply shortage events [14].

PyPSA has been used to develop provincial, multi-node, and hourly optimization models of China's power system. Zhou et al. jointly optimized long-term capacity expansion and operation across 31 provincial-level regions. The analysis covered generation, storage, transmission, and coupling among energy sectors, revealing interactions among renewable variability and flexibility resources [17]. The framework has also been combined with agent-based modeling to examine electricity markets, storage deployment, and low-carbon technology diffusion [38]. More recently, industrial flexible loads have been incorporated into PyPSA-China implementation. The effects of seasonal demand flexibility on system costs and resource allocation were evaluated using provincial-level optimization [39]. These applications primarily address capacity expansion, resource allocation, market design, and demand-side flexibility. These frameworks can already represent thermal power operating constraints. Further comparison can focus on when constraints become binding and how they interact during continuous operation.

System Dynamics represents interactions among electricity supply, demand, generation capacity, and policy through stocks, flows, and feedback loops. It has been used to simulate changes in generation mix and operating conditions under alternative development pathways [40]. Renewable penetration, demand response, and generation investment have also been examined within a common framework. This approach has supported assessments of the long-term effects of policy changes on reliability and renewable development [41]. Hybrid models have already embedded optimization within system dynamics to analyze generation mix trajectories under carbon and capacity policies [42]. Their focus on structural evolution differs from a detailed comparison of constraint activation during continuous hourly operation. For hourly mechanism analysis, the challenge is to preserve chronological constraints while explicitly tracking how successive operating states affect subsequent adjustments.

Supplementary Tables S1 and S2 compare 20 relevant studies in terms of research design, flexibility constraints, scenario settings, evaluation metrics, and principal findings. Collectively, these studies establish links among renewable penetration, net load characteristics, and thermal power flexibility. However, the activation and interaction of minimum stable output, downward ramping, and upward ramping constraints remain insufficiently compared within a consistent chronological framework. To address this gap, this study evaluates these constraints over 8760 consecutive hours and compares individual and combined thermal retrofits under baseline and expanded renewable capacity scenarios. Curtailment and modeled supply shortfalls are assessed under the specified resource configuration and operating rules. The analysis identifies when each constraint becomes relevant and examines the conditions under which retrofit benefits change. The implications for coordination with storage, interregional transmission, and demand-side flexibility are considered within these modeling boundaries.

3. Methodology and Analysis

3.1. Analytical Framework and Constraint Mechanisms

3.1.1. Changes in Renewable Generation and Thermal Power Flexibility Requirements

Wind and solar output is primarily determined by meteorological conditions. As renewable energy penetration increases, the output required from conventional generators is increasingly determined by net load rather than total system load [3]. The net-load definition follows the standard residual-demand approach used in renewable integration and flexibility studies [19,24]. The net load in hour t is expressed as

$$L_{net}(t) = L(t) - P_w(t) - P_v(t) \quad (1)$$

where $L(t)$ denotes the system load in hour t, and $P_w(t)$ and $P_v(t)$ denote the available wind and PV power in the same hour, respectively. As renewable capacity expands, the overall net-load level declines and its hourly variation becomes pronounced [4]. Thermal power units therefore shift from relatively stable generation toward more frequent low-load operation and ramping. These flexibility requirements depend on both the net-load level and its hour-to-hour variation. The former determines turndown requirements, whereas the latter determines ramping requirements. When wind and solar output is high and system load is low, net load falls to a low level. Thermal power units must then reduce their output to create additional room for renewable energy integration. Lower net-load levels therefore require greater turndown capability from thermal power units. Here, all load and generation terms are instantaneous hourly average power (GW); available renewable output refers to generation potential before curtailment.

In addition to the net-load level, changes in net load between consecutive hours determine the system's ramping requirements. The hour-to-hour difference is calculated following established net-load ramping analysis [24,26]. The change in net load in hour t can be expressed as

$$\Delta L_{net}(t) = L_{net}(t) - L_{net}(t-1) \quad (2)$$

where $L_{net}(t-1)$ denotes the net load in hour $t-1$. The absolute value of $\Delta L_{net}(t)$ represents the magnitude of the hour-to-hour change in net load and determines the required ramping capability of thermal power units. A rapid increase in PV generation or a decline in system load causes net load to fall rapidly, creating a downward ramping requirement. By contrast, a decline in PV or wind generation, or a rapid increase in system load, raises net load and creates an upward ramping requirement. A positive net-load change indicates an upward regulation requirement, while a negative change indicates a downward regulation requirement. With a one-hour time step, the difference is expressed in GW per hour when interpreted as a ramp rate.

High renewable energy penetration therefore increases the requirements for both deep turndown and rapid ramping by changing the level and variation of net load. These requirements, however, do not necessarily become binding operating constraints. Whether they become binding depends on the regulating capability actually available in the system. A constraint emerges only when the required thermal output falls below the minimum stable output or when the required hour-to-hour output adjustment exceeds the available ramping capability. Such constraints may limit renewable energy integration or reduce supply reliability. Whether thermal power flexibility becomes a system bottleneck must therefore be assessed on an hourly basis. This requires comparing net-load levels and variations with the feasible output range and ramping capability of thermal power units. Annual or monthly energy balances cannot adequately capture this process.

3.1.2. Mechanisms of Minimum Stable Output and Ramping Constraints

The ability of thermal power units to follow changes in net load is primarily constrained by their minimum stable output and upward and downward ramping capabilities. The minimum stable output determines how far unit output can be reduced, whereas ramping capability determines how much output can change between consecutive hours. These constraints limit the output level and the rate of output adjustment, respectively. Their formation and effects are illustrated in Figure 1.

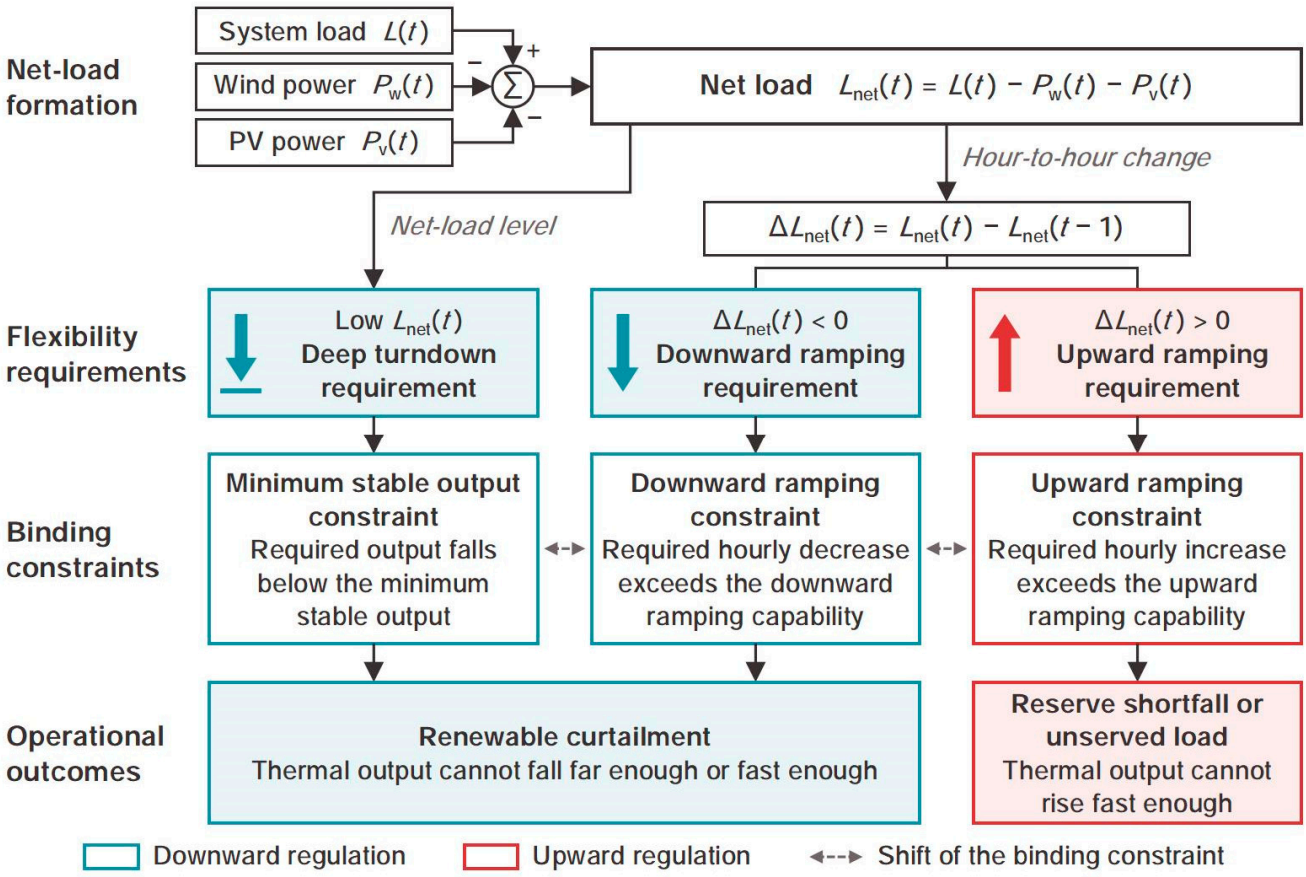


Figure 1. Net-load-driven thermal flexibility requirements, binding constraints, and operational outcomes.

When wind and solar output is high and net load remains low, thermal power units must reduce their output accordingly. If a unit reaches its minimum stable output, no further reduction is possible. This restricts the space available for renewable energy integration. Renewable curtailment may then occur when other flexibility resources are insufficient. Therefore, the minimum stable output constraint mainly reflects insufficient turndown range under low-net-load conditions.

In some periods, however, the main limitation is not the minimum output level but the speed of output reduction. Even when a unit remains above its minimum stable output, it may be unable to reduce generation fast enough. This occurs when the required hour-to-hour output reduction exceeds its downward ramping capability. Renewable curtailment may therefore still occur. The minimum stable output constraint determines whether thermal output can be reduced far enough, whereas the downward ramping constraint determines whether the required reduction can be achieved within the available time.

These two constraints mainly affect renewable energy integration, whereas the upward ramping constraint is more directly related to supply reliability. When renewable generation declines rapidly or system load rises sharply, net load increases. If this increase exceeds the upward ramping capability of thermal power units, thermal generation cannot increase quickly enough. The system reserve margin is then reduced, and unserved load may occur if other flexibility resources are insufficient.

Different constraints may also interact during continuous system operation, and the binding constraint may shift over time. A rapid increase in renewable generation may first trigger the downward ramping constraint. As net load falls further, the minimum stable output constraint may become binding. If renewable generation subsequently declines or system load rises, the upward ramping constraint may become dominant. Hourly analysis can identify when each constraint is triggered and how the dominant constraint changes over time. This provides a mechanistic basis for comparing the effects of different thermal power flexibility retrofit pathways.

3.2. Model Boundaries and Data Processing

The study employs a continuous 8760-h simulation for 2025, covering 31 provincial nodes in China at a 1 h resolution. Chronological simulation preserves consecutive changes in renewable output, demand, and thermal operating conditions that are relevant to system flexibility [13,14]. PyPSA (version 1.2.4) first produces an hourly reference dispatch under the specified generation capacities, resource profiles, storage operation, and interprovincial transmission limits [17]. The system dynamics (SD) model, implemented in Vensim DSS (version 10.4.0), then uses this dispatch as a reference to track how previous-hour thermal output and online capacity affect the feasible output range in each subsequent hour. This coupling supports the comparison of minimum stable output, bidirectional ramp rates, and retrofit coverage under consistent baseline conditions; hybrid optimization–SD approaches provide a methodological precedent [42]. The framework represents coal- and gas-fired generation, nuclear power, conventional hydropower, wind power, solar photovoltaics, pumped-storage hydropower, battery storage, and interprovincial transmission. Table 1 reports the principal numerical inputs and baseline parameters. Figure 2 summarizes the workflow from PyPSA baseline simulation and hourly data transfer to constraint evaluation and scenario comparison.

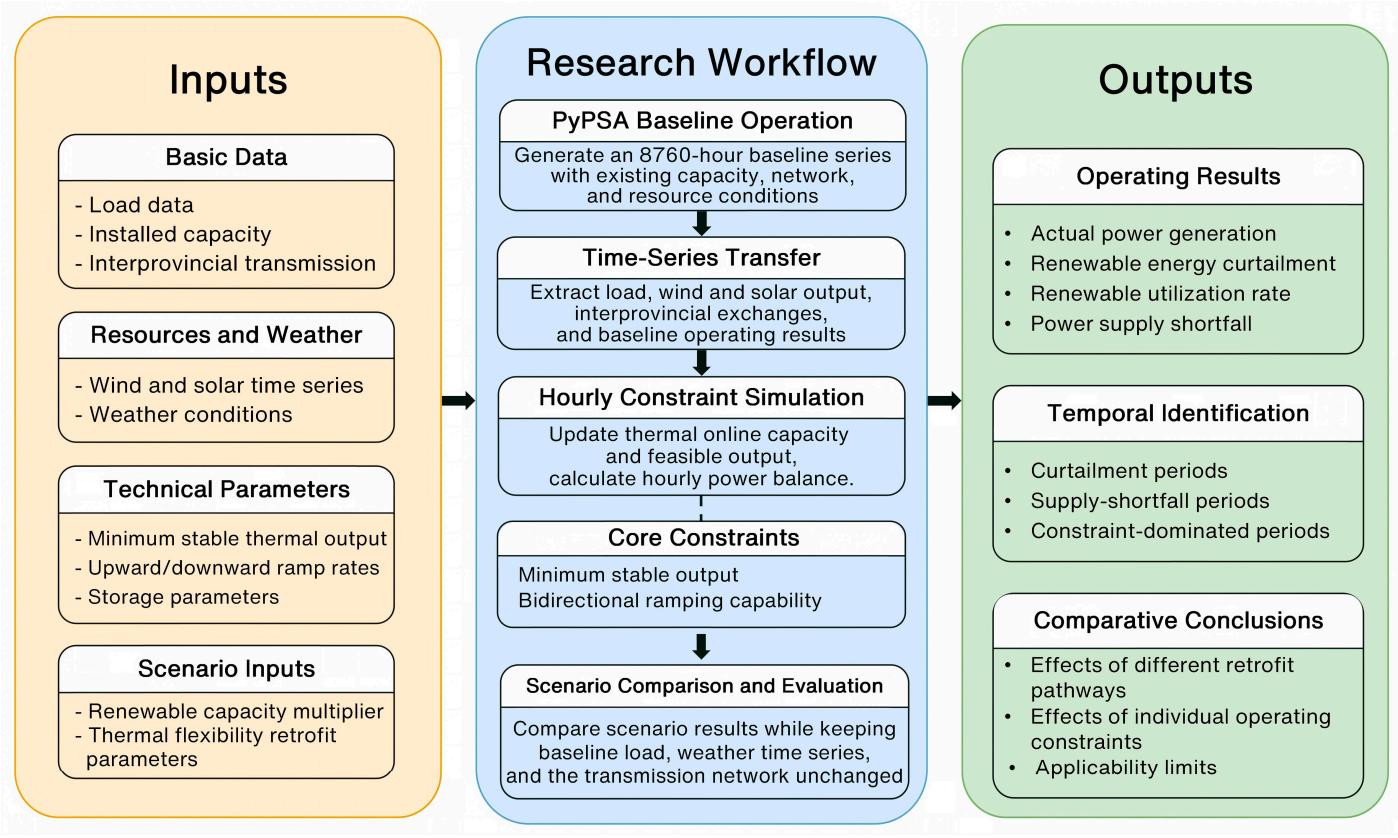


Figure 2. Workflow of the hourly scenario simulation framework. The dashed line indicates the association between the hourly constraint simulation and its core constraints.

Table 1. Numerical Inputs and Baseline Parameters of the Power System Model.

Input Parameter	Baseline Value	Temporal Scale	Spatial Scale	Data Source and Model Treatment
Base year	2025	Annual	National	Model setting
Simulation horizon	8760 h	1 h	National	Continuous full-year hourly simulation
Power system nodes	31	—	Provincial	Each provincial-level region is represented as an individual node
Annual electricity demand	10,368.2 TWh	Annual/hourly	Provincial	Total electricity consumption in 2025; provincial hourly load profiles are used for chronological simulation
Wind power capacity	640.01 GW	Annual/hourly	Provincial	Installed capacity at year-end 2025; onshore and offshore wind are represented separately in the model
Solar PV capacity	1201.73 GW	Annual/hourly	Provincial	Installed capacity at year-end 2025
Nuclear power capacity	62.48 GW	Annual/hourly	Provincial	Installed capacity at year-end 2025
Coal-fired power capacity	1191.07 GW	Annual/hourly	Provincial	Installed capacity at year-end 2025
Gas-fired power capacity	140.00 GW	Annual/hourly	Provincial	Installed capacity at year-end 2025
Conventional hydropower capacity	382.08 GW	Annual	National/provincial	Conventional hydropower capacity at year-end 2025, excluding pumped storage
Pumped-storage capacity	58.69 GW	Annual/hourly	Provincial	Existing capacity stock at year-end 2024 used as the model input; national pumped-storage capacity reached 58.69 GW at year-end 2024

Reference hydropower utilization hours	3367 h	Annual	Provincial	Average utilization hours of large-scale hydropower in 2025, used to define the annual hydropower energy constraint
Wind capacity factors	8760 values per province	1 h	Provincial	Calculated from hourly ERA5 meteorological data using spatial weights derived from the GEM wind-farm database
Solar capacity factors	8760 values per province	1 h	Provincial	Calculated from hourly ERA5 meteorological data using spatial weights derived from the GEM solar-farm database
Baseline minimum stable output of coal-/gas-fired generation	30%/30%	1 h	Provincial	Minimum operating levels of coal- and gas-fired units before flexibility retrofits
Baseline upward ramp rates of coal-/gas-fired generation	60%/90%·h^{-1}	1 h	Provincial	Maximum permissible increase in thermal output between consecutive hours
Baseline downward ramp rates of coal-/gas-fired generation	60%/90%·h^{-1}	1 h	Provincial	Maximum permissible decrease in thermal output between consecutive hours
Maximum hourly start-up capacity shares of coal-/gas-fired generation	10%/30% h^{-1}	1 h	Provincial	Limit the maximum hourly increase in thermal capacity online
Maximum hourly shutdown capacity shares of coal-/gas-fired generation	15%/40% h^{-1}	1 h	Provincial	Limit the maximum hourly decrease in thermal capacity online
Pumped-storage power and energy capacity	59.22 GW/473.77 GWh	Annual/hourly	Provincial	Total capacity represented in the PyPSA baseline simulation
Battery storage power and energy capacity	73.76 GW/168.00 GWh	Annual/hourly	Provincial	Total capacity represented in the PyPSA baseline simulation

Hourly available wind and solar output is calculated from installed capacity and technology-specific capacity factors. These factors are derived from 2025 ERA5 hourly meteorological data and spatially weighted using facility locations reported by Global Energy Monitor (GEM). The PyPSA reference model also accounts for the annual energy limit of conventional hydropower, nuclear availability, storge power and energy limits, and existing interprovincial transfer capacities. Table 1 specifies the capacity parameters and their data sources.

After the PyPSA baseline simulation, hourly nodal load, generation by technology, available wind and solar output, storage charging and discharging power, initial stored energy, and interprovincial power flows are transferred to the SD model. Using PyPSA thermal generation as a reference, the SD model calculates feasible thermal output in each hour from the previous hour's output and online capacity. Feasible output is constrained by minimum stable output, maximum available output, upward and downward ramp rates, and hourly limits on changes in online capacity. Storage dispatch and interprovincial power flows retain their PyPSA baseline schedules. The SD scenarios therefore eval-

uate changes in renewable availability and thermal operating parameters under these retained schedules. They do not re-optimize the entire system for each scenario. The renewable capacity multiplier is applied to available wind and solar output, not to PyPSA's actual renewable generation. In retrofit scenarios, minimum stable output and ramp rates vary by retrofit type and coverage. The baseline scenario uses a renewable capacity multiplier of 1.00 and no thermal retrofit.

At baseline, available wind and solar energy is 3165.62 TWh in both models. Actual wind and solar generation is 2888.12 TWh in PyPSA and 2892.23 TWh in the SD model; the corresponding curtailment is 277.50 and 273.39 TWh. The SD estimate of actual generation is approximately 0.14% higher than the PyPSA value. PyPSA reports no unserved energy, whereas the SD model reports 0.0025 MWh, which is treated as a numerical residual. This comparison establishes close agreement in annual energy totals and supply balance, but does not imply identical hourly dispatch. The reported 2025 utilization rates were 94% for wind power and 95% for solar photovoltaics [43]. These technology-specific figures differ from the modelled combined wind-and-solar utilization rate of 91.4%. Because interprovincial transfer capacity is represented using available public data, the baseline is used for scenario comparisons rather than as an estimate of observed national curtailment.

3.3. Hourly Thermal Operating Constraints and Power Balance

The SD model uses the hourly PyPSA dispatch as a reference and calculates thermal generation and the resulting power balance in chronological order. For each province and thermal technology, online capacity in the current hour is determined by online capacity in the preceding hour, capacity started, and capacity shut down. Hourly limits constrain both changes in online capacity. The previous hour's generation and online capacity then determine the feasible output range in the current hour. Thermal output therefore depends on both current net demand and the preceding operating state.

The minimum stable output is determined by online capacity and the minimum stable output ratio [13,36]:

$$P_{i,g,t}^{phys,\min} = C_{i,g,t}^{on} \mu_g \tag{3}$$

where $C_{i,g,t}^{on}$ denotes the online capacity of thermal power technology g in province i at hour t, and μ_g denotes the minimum stable output ratio. Reducing μ_g expands the static downward operating range. Whether a unit can reach the lower output within a given hour also depends on its downward ramping capacity.

The effective lower and upper output bounds combine the physical operating range with the preceding hour's generation and the bidirectional ramp rates [13,36]:

$$P_{i,g,t}^{eff,\min} = \max\left(P_{i,g,t}^{phys,\min}, P_{i,g,t-1}^{th} - r_g^{\downarrow} C_{i,g,t-1}^{on} \Delta t\right) \tag{4}$$

$$P_{i,g,t}^{eff,\max} = \min\left(P_{i,g,t}^{phys,\max}, P_{i,g,t-1}^{th} + r_g^{\uparrow} C_{i,g,t}^{on} \Delta t\right) \tag{5}$$

In Equations (4) and (5), $P_{i,g,t-1}^{th}$ is actual thermal generation in the preceding hour, and $P_{i,g,t}^{phys,\max}$ is the physical maximum available output in the current hour. $r_g^{\downarrow}$ and $r_g^{\uparrow}$ are the downward and upward ramp rates, and $\Delta t = 1h$. Consistent with the implemented model, the downward ramp allowance is based on online capacity in the preceding hour, whereas the upward allowance is based on online capacity in the current hour.

Required thermal output below the effective lower bound may increase renewable curtailment. Required output above the effective upper bound may contribute to unserved demand.

The model first adjusts PyPSA reference thermal generation to the feasible output range. Any further adjustment is allocated between coal- and gas-fired generation according to their available operating headroom. Under a deep-turndown retrofit, recoverable baseline curtailment is limited by PyPSA baseline curtailment, the reduction in effective minimum thermal output, and contemporaneous demand that can absorb additional wind and solar generation. The minimum-output violation is calculated first, and the downward-ramping violation is measured after this component has been separated. Curtailment associated with thermal constraints is allocated between these components in proportion to their calculated magnitudes. An analogous allocation is applied to unserved demand associated with capacity and upward-ramping constraints. Attributed curtailment and unserved demand are each capped by their respective actual totals, with any remainder reported separately. These attribution shares are diagnostic measures, not independent estimates of the benefit from removing each constraint.

Figure 3 presents the stock–flow structure of thermal power operation and flexibility adjustment. Online capacity and actual output in the preceding hour determine the current operating state and the feasible output bounds. Coal- and gas-fired output adjustments are then allocated within these bounds using PyPSA baseline generation as the reference. Minimum stable output, ramp rates, and retrofit coverage affect final thermal output by changing the feasible operating range.

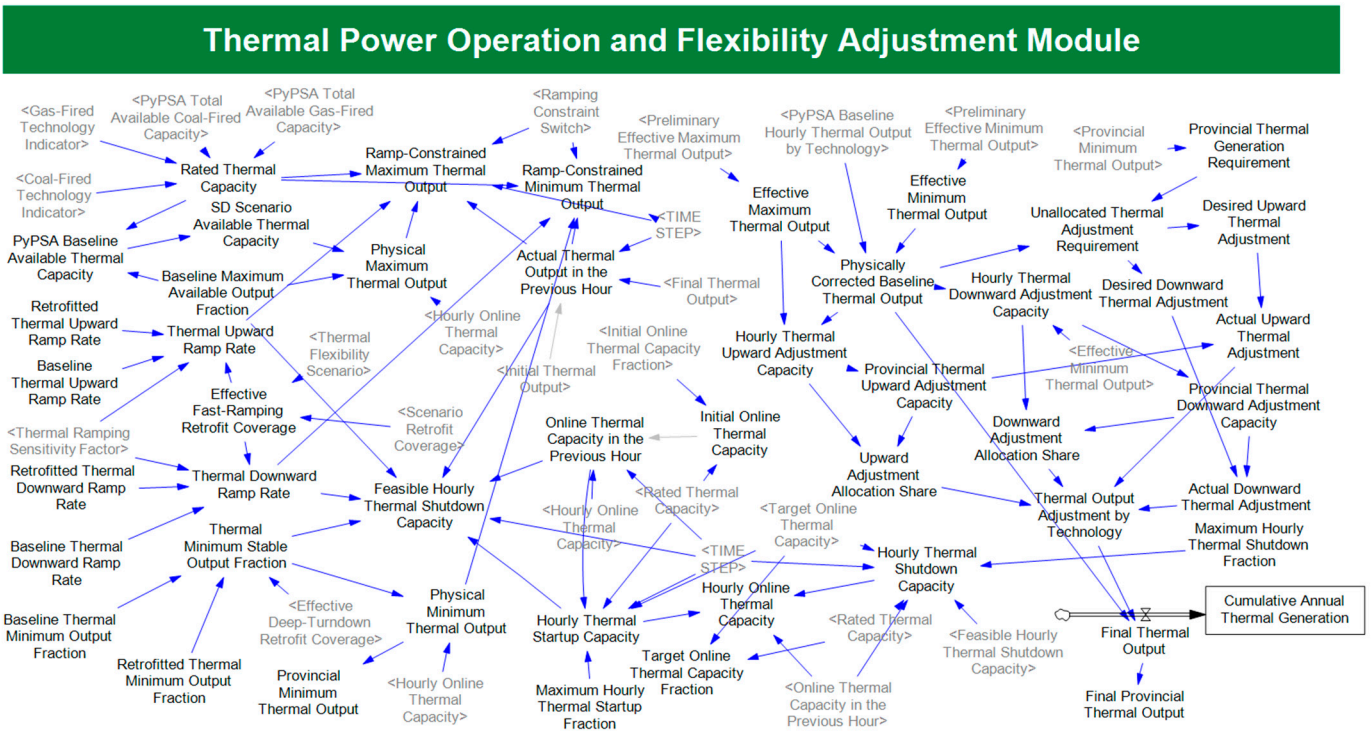


Figure 3. Stock–flow structure of the thermal power operation and flexibility adjustment module. Grey text in angle brackets denotes shadow variables referencing variables defined elsewhere in the model. Grey arrows indicate initialization dependencies, blue arrows indicate information dependencies, and black pipe arrows represent flows into stocks.

In the PyPSA baseline, pumped-storage hydropower and battery energy storage are dispatched subject to power, energy, efficiency, and state-of-charge constraints. No separate evening-peak state-of-charge reservation rule is applied in the SD scenarios. The SD

model retains the resulting hourly charging and discharging schedules across scenarios and updates stored energy to check the energy balance [44]:

$$E_{i,s,t} = E_{i,s,t-1} + \eta_s^{ch} P_{i,s,t}^{ch} \Delta t - \frac{P_{i,s,t}^{dis}}{\eta_s^{dis}} \Delta t \quad (6)$$

where $E_{i,s,t}$ denotes the stored energy of storage technology S. P^{ch} and P^{dis} denote the charging and discharging power, respectively, and η^{ch} and η^{dis} denote the charging and discharging efficiencies, respectively. In the scenarios examined here, initial stored energy and hourly charging and discharging power are taken from the PyPSA baseline results. Stored energy is measured in GWh, charging and discharging powers in GW, and the charging and discharging efficiencies are dimensionless. Charging increases stored energy after efficiency losses, whereas discharging decreases it after accounting for conversion losses; the hourly time step is 1 h.

After thermal generation is adjusted and renewable curtailment is determined, Equation (7) describes the hourly power balance for each province [13,14]:

$$L_{i,t} = P_{i,t}^{th} + P_{i,t}^{nonth} + P_{i,t}^{sto} + P_{i,t}^{netimp} + P_{i,t}^{uns} \quad (7)$$

L is demand. P^{th} is actual thermal generation. P^{nonth} comprises nuclear power, hydropower, and actual wind and solar generation after curtailment. P^{sto} is storage discharge minus charging, P^{netimp} is net interprovincial imports, and $U \geq 0$ is residual unserved demand. Positive net storage output and positive net imports both increase supply available to the province. The difference between available and actual wind and solar generation is recorded as curtailment. Equation (8) calculates annual renewable utilization from annual available generation and curtailment [19].

$$UR = 1 - \frac{\sum_{i,t} P_{i,t}^{curt} \Delta t}{\sum_{i,t} P_{i,t}^{ava} \Delta t} \quad (8)$$

where $P_{i,t}^{curt}$ and $P_{i,t}^{ava}$ denote renewable energy curtailment power and available renewable energy output, respectively. Both quantities are non-negative hourly power values in GW. The utilization rate is dimensionless; for annual reporting, the corresponding hourly energy terms are summed before calculating the ratio. This is the renewable generation utilization measure used in integration studies [19].

Figure 4 shows how available wind and solar output enters the hourly power balance and is converted into actual generation or curtailment. Load, nuclear and hydropower output, final thermal output from Figure 3, storage net output, and net imports jointly determine the hourly surplus or shortfall. The model then calculates wind and solar generation, curtailment, and unserved load and identifies the associated operating constraints. Storage net output and net imports retain their hourly PyPSA baseline schedules across scenarios.

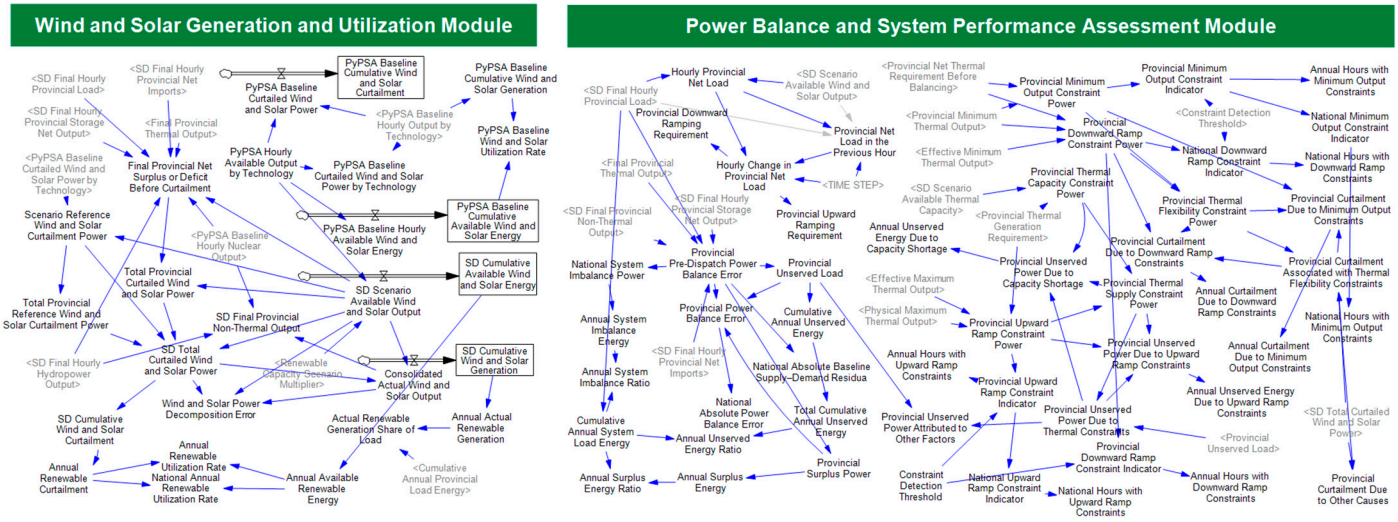


Figure 4. Stock–flow structure of the wind and solar integration and power balance module. Grey text in angle brackets denotes shadow variables referencing variables defined elsewhere in the model. Grey arrows indicate initialization dependencies, blue arrows indicate information dependencies, and black pipe arrows represent flows into stocks.

Accordingly, the model links hourly changes in renewable output and demand to thermal operating constraints, renewable curtailment, and modeled supply shortfalls. Using the PyPSA baseline as a common reference, the SD layer updates online thermal capacity through hourly startup and shutdown flows. Previous-hour thermal output and online capacity determine the feasible output range in the current hour. The model records constraint activation and calculates associated curtailment, unserved energy, and renewable utilization. Retrofit scenarios change the feasible output range through minimum stable output, bidirectional ramp rates, and retrofit coverage. Here, SD serves as an hourly stock–flow scenario simulation rather than a model of endogenous investment or policy feedback. Its role is to make inter-hour adjustments and constraint attribution explicit, not to introduce operating constraints unavailable in PyPSA.

3.4. Scenario Design

Four sets of scenarios are defined to distinguish the effects of renewable capacity expansion and thermal power flexibility retrofits: a baseline, renewable capacity scenarios, thermal flexibility scenarios, and combined scenarios (Table 2). The baseline has wind and solar capacity multipliers of 1.00 and no thermal retrofit. It is denoted R0 or S0. All scenarios use the same hourly demand, wind and solar resource profiles. Nuclear, hydropower, and other non-scenario inputs remain unchanged. Storage charging and discharging and interprovincial transfer follow the hourly PyPSA baseline schedules.

Table 2. Renewable energy capacity and thermal power flexibility scenario settings.

Scenario Type	Scenario	Renewable Energy Capacity Multiplier	Thermal Power Flexibility Retrofit	Minimum Stable Output Ratio (Coal/Gas)	Upward Ramp Rate (Coal/Gas)	Downward Ramp Rate (Coal/Gas)	Retrofit Coverage
Baseline scenario	R0/S0	1.00	No flexibility retrofit	30%/30%	60%/90%·h^{-1}	60%/90%·h^{-1}	0
Renewable energy capacity scenarios	R1	1.25	No flexibility retrofit	30%/30%	60%/90%·h^{-1}	60%/90%·h^{-1}	0
	R2	1.50					
	R3	1.75					
	R4	2.00					

Thermal power flexibility scenarios	S1	1.00	Deep peak-shaving retrofit	25%/25%	60%/90%·h^{-1}	60%/90%·h^{-1}	50%
	S2		Fast-ramping retrofit	30%/30%	120%/180%·h^{-1}	120%/180%·h^{-1}	50%
	S3		Integrated flexibility retrofit	25%/25%	120%/180%·h^{-1}	120%/180%·h^{-1}	50%
	S4		Expanded integrated retrofit	22%/22%	156%/234%·h^{-1}	156%/234%·h^{-1}	80%
Combined scenarios	R2S0–R2S4	1.50	Apply S0–S4, respectively	Adjust according to the corresponding S scenario	Adjust according to the corresponding S scenario	Adjust according to the corresponding S scenario	0–80%
	R4S0–R4S4	2.00					

In R1–R4, wind and solar capacities are increased together to 1.25, 1.50, 1.75, and 2.00 times their baseline levels, while thermal operating parameters remain at R0 values. Equal increments allow the additional available renewable energy to be compared with changes in actual generation and curtailment. The combined scenarios pair S0–S4 with R2 and R4 to examine retrofit effects at intermediate and high levels of renewable expansion. These multipliers are system stress-test assumptions, not forecasts of future installed capacity.

The thermal flexibility scenarios vary the minimum stable output ratio and upward and downward ramp rates. In the PyPSA baseline, the minimum stable output ratio is 30% of rated capacity for both coal- and gas-fired generation. The SD baseline sets the coal- and gas-fired ramp rates at 60% and 90% of rated capacity per hour, respectively. These values correspond to 1.0% and 1.5% of rated capacity per minute. The baseline coal-fired ramp rate follows a previous scenario study of China's power system [4]. S1 applies a deep peak-shaving retrofit, S2 applies a fast-ramping retrofit, and S3 combines both, each at 50% coverage. S4 examines a broader combined-retrofit case at 80% coverage. Retrofit coverage denotes the assumed share of coal- and gas-fired capacity assigned the retrofit target parameters. This share is applied uniformly across provincial nodes; individual generating units are not selected, and no provinces are prioritized. The effective operating parameters reflect the baseline values, retrofit target values, and assumed coverage. S4 is an exploratory high-coverage scenario, not a projection of achievable retrofit deployment.

To assess the influence of the baseline ramp-rate assumption, only the upward and downward ramp rates of coal-fired generation were varied under the unretrofitted R0/S0 conditions; all other inputs were held constant. A0 used the baseline rate of 60% of rated capacity per hour. A1, A2, and A3 used 48%, 72%, and 90% per hour, respectively, with A1 serving as a lower-rate stress test. Relative to A0, A1 increased annual curtailment by 3.519 TWh and produced 5.010 TWh of unserved energy. Curtailment decreased by only 0.005 and 0.007 TWh in A2 and A3, respectively, while unserved energy remained negligible. Under the 1 h resolution and operating limits used here, increases above the baseline rate had little effect on annual outcomes, whereas reducing the rate to 48% per hour substantially affected supply balance. This test concerns the baseline parameter assumption and is separate from the retrofit scenarios in Table 2.

4. Results

4.1. Isolated Effects of Renewable Capacity Expansion

To isolate the effect of renewable capacity expansion, installed wind and solar capacity was scaled stepwise from 1.00 to 2.00 across scenarios R0–R4. Thermal flexibility parameters and other system conditions were held constant. Annual available wind and solar energy increased with capacity, but the additional energy was not converted proportionally into actual generation. Available energy rose from 3165.6 TWh in R0 to 6331.2 TWh in R4. Actual generation increased from 2892.2 to 4379.5 TWh, a gain of 51.4%. Over

the same scenarios, curtailment rose from 273.4 to 1951.7 TWh (Figure 5a). Of the additional 3165.6 TWh available in R4, 1487.3 TWh was converted into actual generation and 1678.4 TWh was curtailed. These amounts accounted for 47.0% and 53.0% of the increase in available energy, respectively.

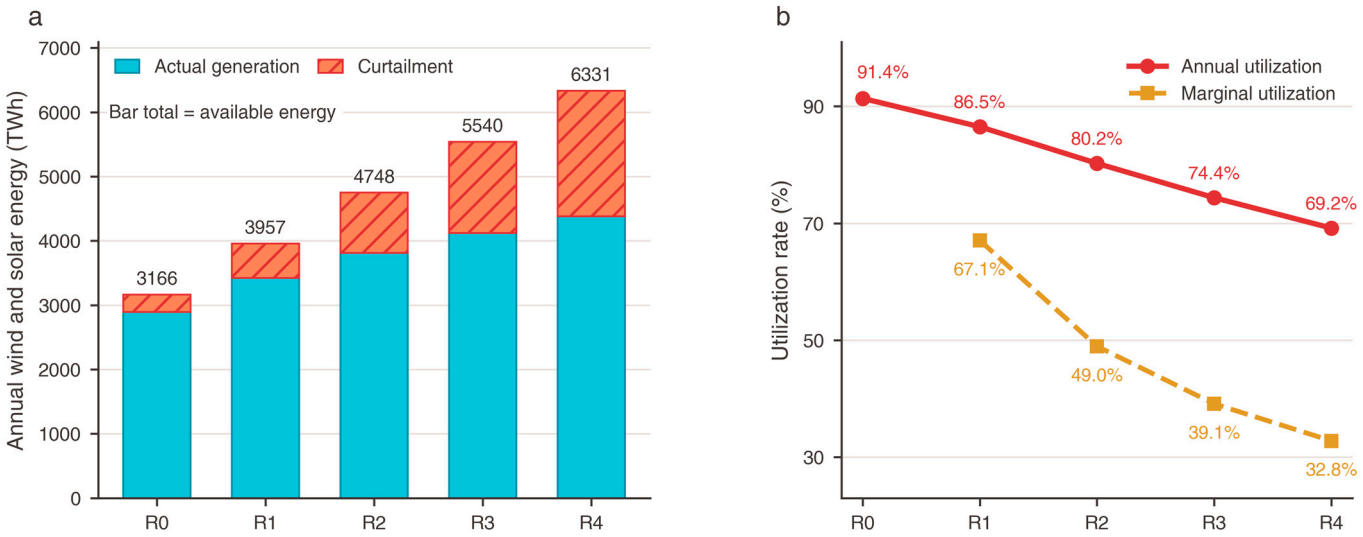


Figure 5. Effects of renewable capacity expansion on annual wind and solar energy and utilization. (**a**) Actual generation and curtailment under scenarios R0–R4. The value above each stacked bar represents total available energy, equal to actual generation plus curtailment. (**b**) Annual utilization rate and marginal utilization rate. Marginal utilization is calculated between adjacent scenarios and is therefore not defined for R0.

Renewable energy utilization declined as installed capacity increased. The annual utilization rates for R0–R4 were 91.4%, 86.5%, 80.2%, 74.4%, and 69.2%, respectively. This represented a decrease of 22.2 percentage points between the baseline and highest-capacity scenarios (Figure 5b). To distinguish average utilization from the contribution of additional capacity, a marginal utilization rate was calculated for each consecutive scenario pair. It was defined as the increase in actual generation divided by the increase in available energy. The marginal rates for R0–R1, R1–R2, R2–R3, and R3–R4 were 67.1%, 49.0%, 39.1%, and 32.8%, respectively. Available energy increased by approximately 791.4 TWh at each step. However, the increase in actual generation fell from 530.7 TWh in the first step to 259.5 TWh in the last. The corresponding increase in curtailment rose from 260.7 to 531.9 TWh. Under unchanged system flexibility conditions, additional capacity therefore produced progressively less actual generation per unit of additional available energy.

The hourly results revealed when the increase in curtailment occurred. Mean curtailed power was calculated for each hour of the day across the full year (Figure 6a). In every scenario, curtailment rose during the morning, peaked at approximately 13:00, and declined thereafter. The midday peak increased with installed capacity. It was approximately 150 GW in R0 and nearly 790 GW in R4. Mean curtailed power was lower at night and in the early morning, when differences among scenarios were also smaller. With capacity expansion, the midday profile rose and high curtailment persisted over more hours. The annual increase was thus concentrated in particular hours rather than distributed uniformly throughout the year.

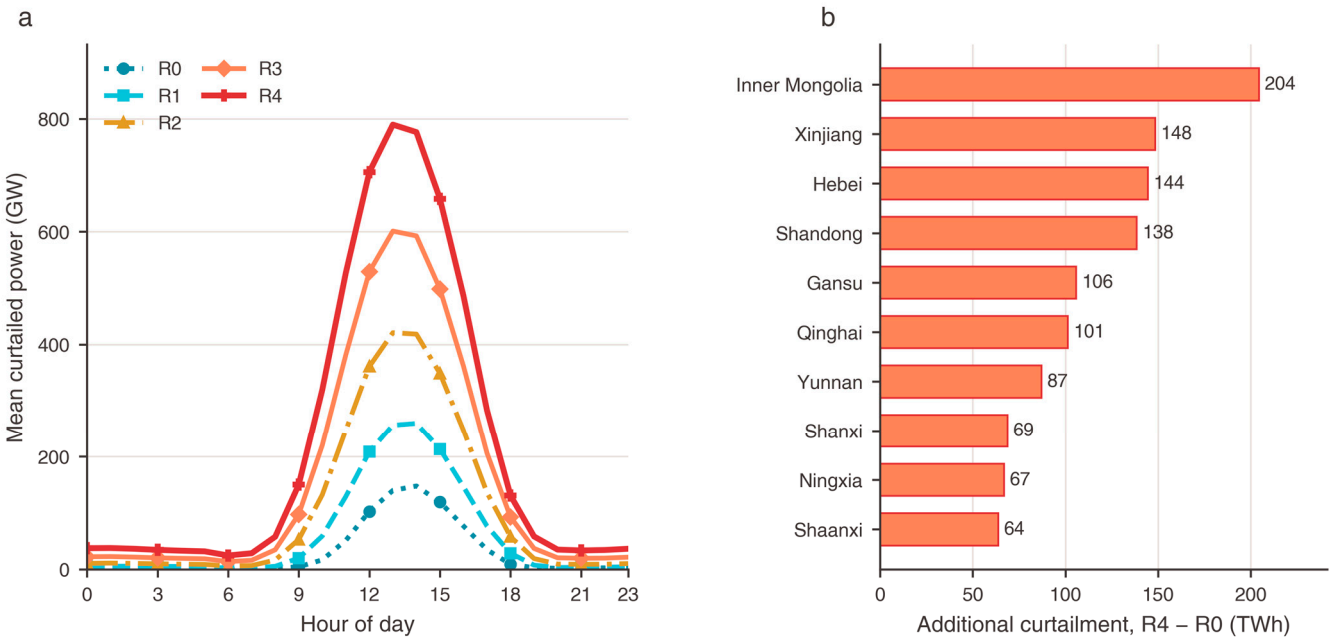


Figure 6. Intraday distribution and regional variation in curtailment under renewable capacity expansion. (**a**) Annual mean curtailed power by hour of day in R0–R4; (**b**) the 10 provincial-level regions with the largest increases in curtailment from R0 to R4.

Additional curtailment was also unevenly distributed across regions. Provincial increases between R0 and R4 are compared in Figure 6b. Curtailment increased by approximately 204 TWh in Inner Mongolia, 148 TWh in Xinjiang, 144 TWh in Hebei, 138 TWh in Shandong, and 106 TWh in Gansu. Together, these five regions accounted for approximately 740 TWh, or 44% of the national increase. Curtailment also rose in other regions, but their absolute increases differed substantially. The national utilization rate therefore concealed the concentration of additional curtailment across both hours and regions. Annual energy totals, hourly power profiles, and regional contributions should be considered together when assessing the operating effects of capacity expansion.

4.2. Isolated Effects of Thermal Power Flexibility Retrofits

With the renewable capacity multiplier fixed at 1.00, scenarios S0–S4 were compared to isolate the effects of different thermal power flexibility retrofits. No retrofit was applied in S0. Minimum stable output was reduced in S1, while upward and downward ramp rates were increased in S2. Both measures were applied in S3. Retrofit coverage was set at 50% in S1–S3. In S4, the combined retrofit used the same target parameters as S3, but its coverage increased from 50% to 80%. This increased coverage changed the coverage-weighted effective operating parameters.

The retrofit pathways had markedly different effects on renewable energy utilization. In S0, actual renewable generation was 2892.2 TWh, curtailment was 273.4 TWh, and the utilization rate was 91.4%. Following the deep-turndown retrofit in S1, actual generation increased to 2917.3 TWh. Curtailment fell to 248.4 TWh, a reduction of 25.0 TWh, or 9.2%, relative to S0. By contrast, increasing ramp rates alone in S2 reduced annual curtailment by only approximately 0.007 TWh. Actual generation and the utilization rate remained nearly unchanged from S0. Curtailment in S3 was 248.3 TWh, approximately 0.06 TWh below that in S1. Thus, at 50% retrofit coverage, adding ramp-rate improvements provided little additional annual curtailment reduction. In S4, curtailment declined further to 234.9 TWh, while actual generation rose to 2930.7 TWh. The utilization rate reached 92.6%. Compared with S0, curtailment was reduced by 38.5 TWh, or 14.1% (Figure 7a).

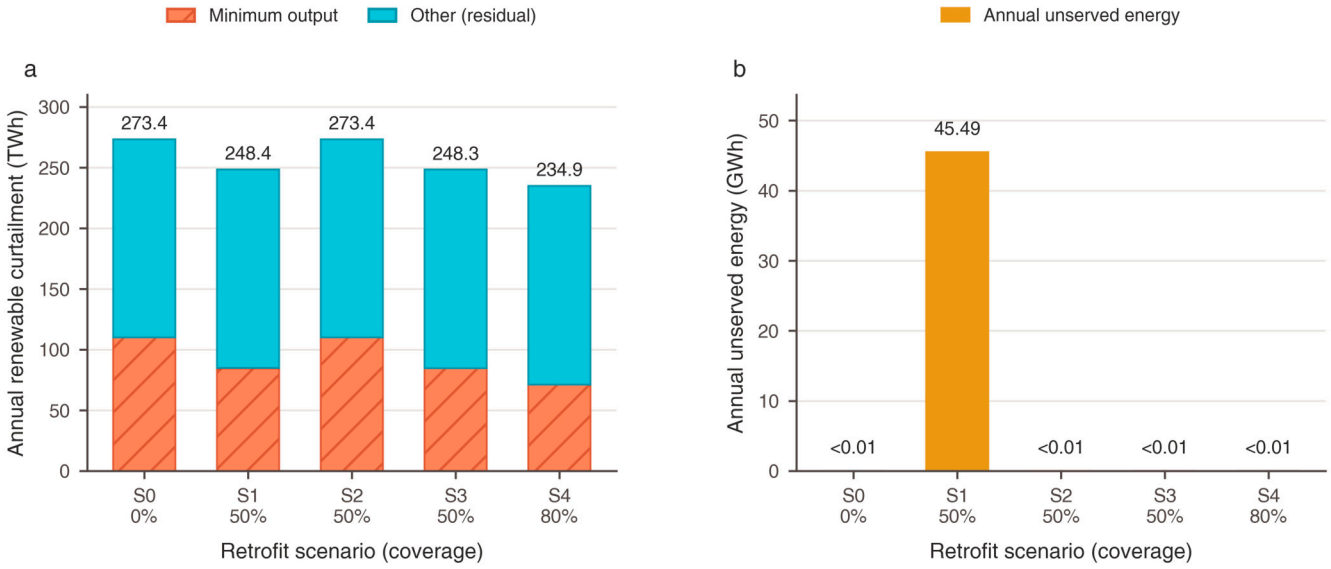


Figure 7. Attribution of renewable curtailment and unserved energy under thermal power flexibility retrofits. (**a**) Annual curtailment and its attribution to operating constraints in S0–S4; (**b**) annual unserved energy.

The attribution of curtailment to operating constraints was consistent with these scenario differences. Annual curtailment attributed to the minimum-stable-output constraint declined from 110.1 TWh in S0 to 84.8 TWh in S1. It fell further to 71.2 TWh in S4. In S2, curtailment attributed to the downward-ramping constraint decreased from approximately 0.049 to 0.001 TWh. This constraint accounted for little curtailment in the baseline, so its relaxation had limited effect on total curtailment. Under the capacity and operating conditions examined, lowering minimum stable output yielded a greater annual utilization benefit than increasing ramp rates alone.

Improvements in renewable utilization were not always accompanied by improvements in supply reliability. Annual unserved energy was close to zero in S0, S2, S3, and S4. By contrast, 45.49 GWh of unserved energy was recorded in S1 (Figure 7b). The model attributed this shortfall to the upward-ramping constraint rather than insufficient installed capacity. When ramp-rate improvements were added to deep turndown in S3, unserved energy approached zero. The curtailment reduction remained close to that achieved in S1. Thus, although a lower thermal output limit increased renewable accommodation, upward adjustment capability remained important in subsequent hours.

The hourly profiles identified when these effects occurred. Mean curtailed power peaked around midday in every scenario, and the timing of the peak changed little after retrofitting. The S0 and S2 profiles nearly overlapped, as did those of S1 and S3. Midday curtailment was lowest in S4 (Figure 8a). The additional unserved energy in S1 was concentrated at 18:00–19:00. At 18:00, the cumulative shortfall over the year was approximately 27.0 GWh. The shortfall at the same hour was nearly eliminated in S3 (Figure 8b). The utilization benefit of deep turndown was therefore concentrated around midday, whereas the shortfall associated with deep turndown alone occurred mainly in the evening.

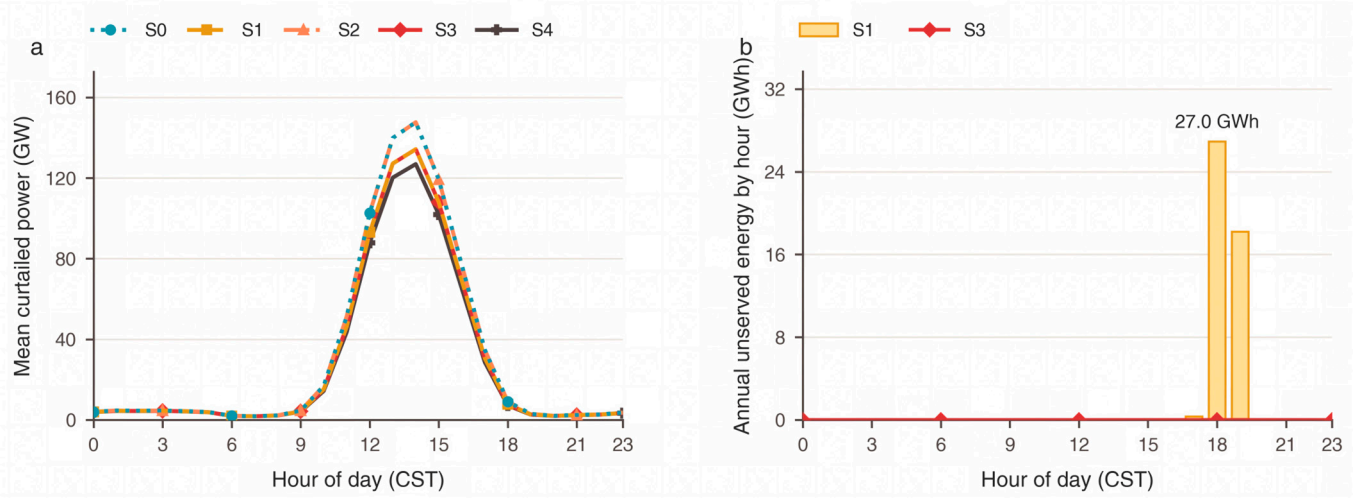


Figure 8. Effects of thermal power flexibility retrofits on the intraday distribution of curtailment and unserved energy. (**a**) Annual mean curtailed power by hour of day in each scenario; (**b**) annual unserved energy in S1 and S3, aggregated by hour of day.

Retrofit benefits also varied across regions. Relative to S0, curtailment in S4 was reduced by approximately 8.16 TWh in Xinjiang, 6.41 TWh in Inner Mongolia, 5.97 TWh in Shanxi, and 5.21 TWh in Shandong. These four regions accounted for approximately 67% of the national reduction (Figure 9b). The utilization rate increased by 5.57 percentage points in Shanxi and 4.39 percentage points in Ningxia, while smaller changes were observed in some other regions (Figure 9a). Thus, even under the same scenario parameters, the annual utilization benefit of thermal flexibility retrofits differed substantially across regions.

4.3. Combined Effects of Renewable Capacity Expansion and Thermal Power Flexibility Retrofits

The S0–S4 thermal flexibility retrofits were applied at renewable capacity multipliers of 1.50 and 2.00. R2S0 and R4S0 corresponded to the no-retrofit R2 and R4 scenarios, respectively. They served as reference cases for assessing retrofit effects at each capacity level. Available wind and solar energy was held constant within each group. Consequently, increases in actual generation corresponded to reductions in curtailment.

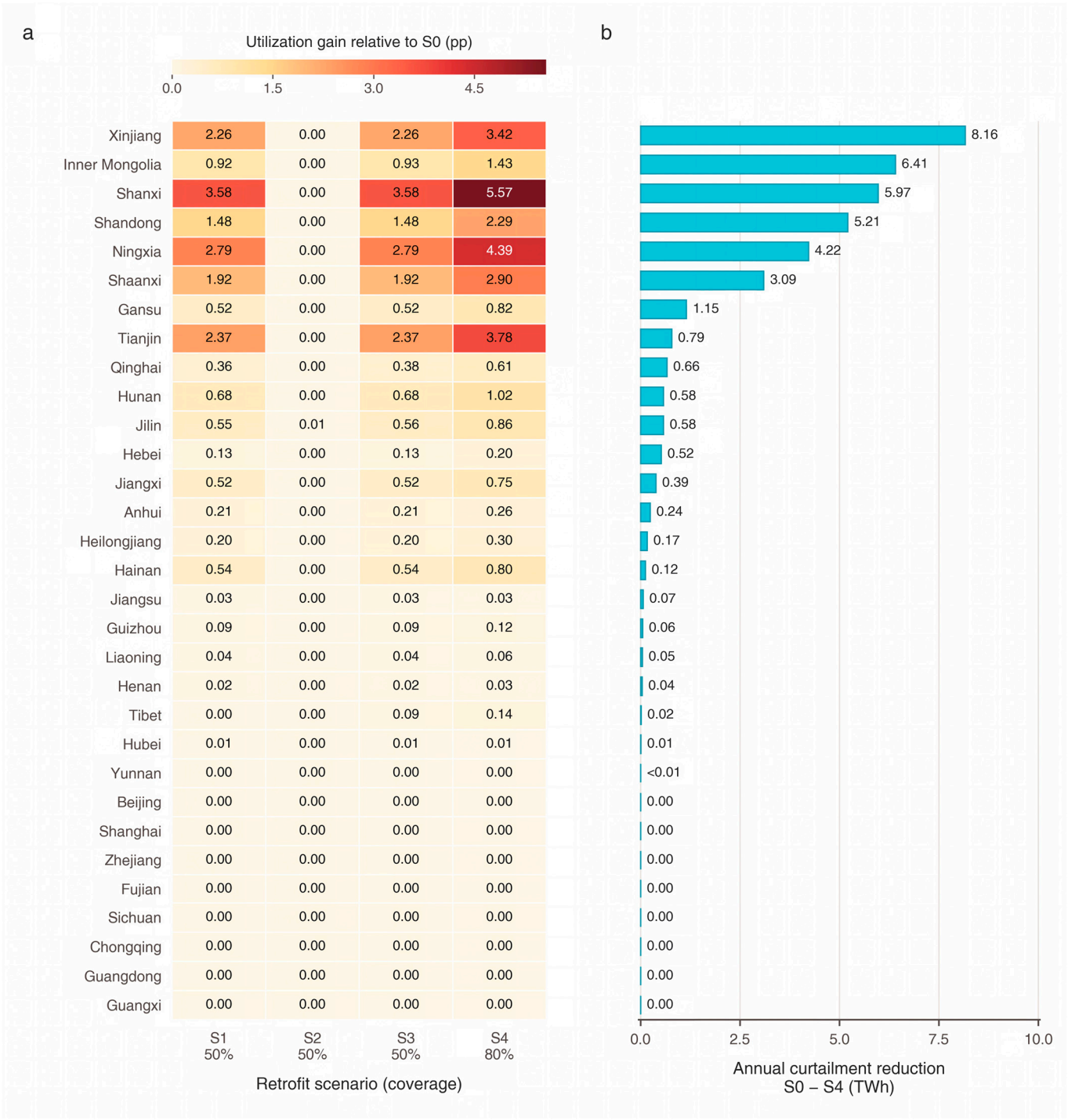


Figure 9. Provincial variation in the renewable utilization effects of thermal power flexibility retrofits. (**a**) Provincial increases in utilization rate relative to S0 under each retrofit scenario; (**b**) provincial reductions in annual curtailment in S4 relative to S0.

The combined retrofit reduced annual curtailment at both capacity levels, although its absolute and relative effects differed. In the R2 group, curtailment declined from 938.0 TWh in R2S0 to 782.5 TWh in R2S4. This was a reduction of 155.5 TWh, or 16.6%. Actual renewable generation increased from 3810.4 to 3966.0 TWh, and the utilization rate rose from 80.2% to 83.5%. In the R4 group, S4 reduced curtailment from 1951.7 to 1760.0 TWh, a reduction of 191.7 TWh, or 9.8%. Actual generation increased from 4379.5 to 4571.2 TWh, while the utilization rate rose from 69.2% to 72.2% (Figure 10a). The relative curtailment reduction was 14.1% at the baseline capacity level, 16.6% in R2, and 9.8% in R4. Thus,

absolute curtailment savings increased across the capacity levels examined, but the relative reduction was not monotonic. The relative effect was smaller in R4 than in R2.

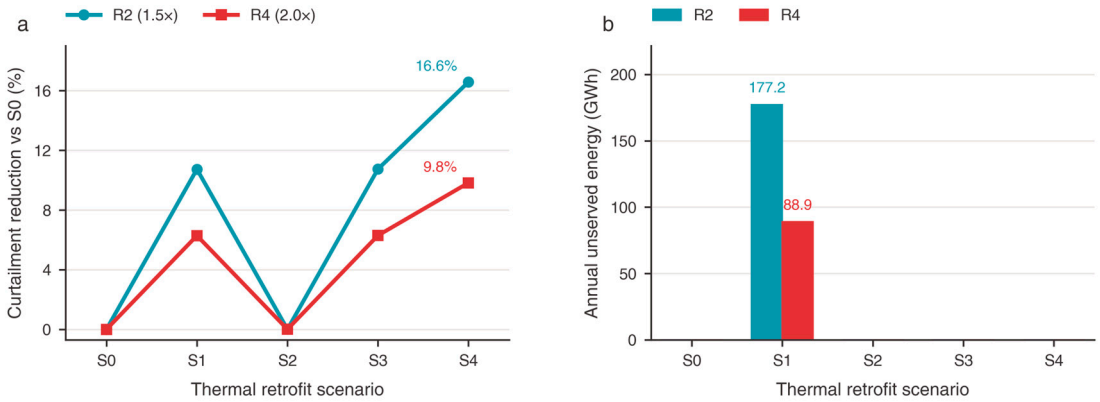


Figure 10. Annual operating outcomes under combined renewable capacity and thermal flexibility scenarios. (**a**) Curtailment reduction rates for each retrofit relative to S0 within the R2 and R4 groups; (**b**) annual unserved energy under each combined scenario.

The effects also differed among retrofit pathways. Deep turndown alone in S1 reduced curtailment by 100.7 TWh in the R2 group and 122.7 TWh in the R4 group. By comparison, ramp-rate improvements alone in S2 reduced curtailment by only approximately 0.04 and 0.14 TWh, respectively. When ramp-rate improvements were added to deep turndown in S3, annual curtailment remained close to the S1 level in both groups. Further reductions were achieved under the expanded combined retrofit in S4 (Figure 10a). Under the specified capacity levels and baseline parameters, lower minimum stable output accounted for most of the annual curtailment reduction. Increasing ramp rates alone had little effect on total curtailment.

Curtailment benefits were assessed alongside unserved energy. Annual unserved energy was close to zero in R2S0 and R4S0. Under S1, however, it reached 177.2 GWh in the R2 group and 88.9 GWh in the R4 group. It remained close to zero under S2, S3, and S4 (Figure 10b). The S1 shortfalls were concentrated at 18:00–19:00 and were larger in R2 than in R4 (Figure 11b). Compared with S1, S3 retained a similar curtailment reduction while eliminating the shortfall. This difference shows the reliability effect of adding ramp-rate improvements. Unserved energy did not increase monotonically as the capacity multiplier rose from 1.50 to 2.00.

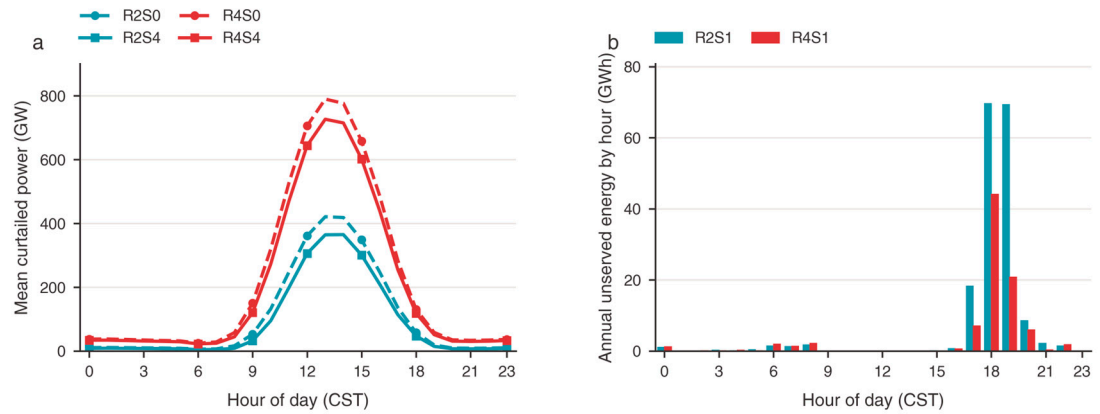


Figure 11. Intraday distribution of renewable curtailment and unserved energy under combined scenarios. (**a**) Annual mean curtailed power by hour of day in R2S0, R2S4, R4S0, and R4S4; (**b**) annual unserved energy in R2S1 and R4S1, aggregated by hour of day.

The hourly profiles showed that the combined retrofit mainly reduced midday curtailed power without changing when curtailment was concentrated. Mean curtailed power peaked at approximately 13:00 in both R2S0 and R4S0. Under S4, the midday profiles declined in both groups. Nevertheless, curtailed power at and around the peak remained substantially higher in R4S4 than in R2S4 (Figure 11a). This pattern was consistent with the annual results. Although curtailment in R4S4 was 191.7 TWh below that in R4S0, 1760.0 TWh remained.

To examine how the evening shortfall arises under S1, Figure 12 presents an hourly operating sequence for Shandong on 23 January 2025. This case exhibits both reduced midday curtailment and an evening supply shortfall. In the R2 and R4 groups, S1 reduced midday thermal output and wind and solar curtailment relative to S0. At 18:00, required thermal output reached 93.28 GW in R2S1 and 92.43 GW in R4S1. The maximum output feasible under the upward-ramping constraint was 88.91 GW in both cases, leaving modeled shortfalls of 4.37 and 3.52 GW, respectively. Physical maximum thermal output was 94.14 GW in both groups and exceeded the required output. The shortfall was therefore associated with the rate of output recovery rather than insufficient available capacity. Under S3, the shortfall at this hour was nearly eliminated. This case illustrates how deep turndown can create room for renewable generation at midday while increasing the subsequent requirement for upward adjustment.

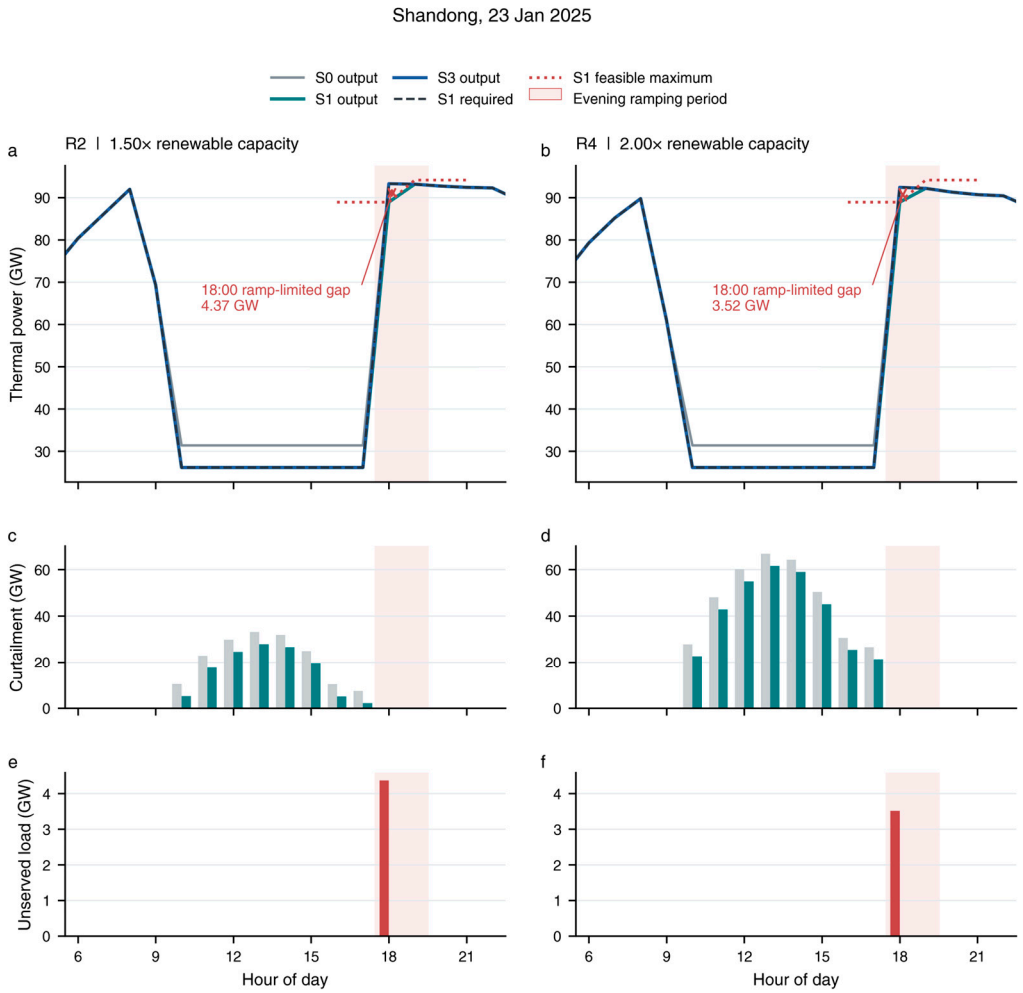


Figure 12. Hourly thermal output, renewable curtailment, and supply shortfalls under combined scenarios. Hourly results for Shandong on 23 January 2025. (**a**,**b**) Actual thermal output under S0, S1, and S3, together with required thermal output and the ramp-constrained feasible maximum under S1, for the R2 and R4 groups, respectively. (**c**,**d**) Wind and solar curtailment under S0 and S1.

(**e**,**f**) Modeled unserved load under S1 and S3. The selected day illustrates a high-shortfall event and does not represent an annual average. Red shading highlights the evening ramping period from 17:30 to 19:30.

Retrofit benefits also varied by region. In the R2 group, the largest curtailment reductions under S4 relative to S0 were recorded in Shandong, Xinjiang, Shanxi, and Inner Mongolia. The respective reductions were 17.71, 16.58, 13.42, and 13.21 TWh (Figure 13a). In the R4 group, the reduction in Shandong rose to 20.01 TWh. The corresponding values for Xinjiang, Shanxi, and Inner Mongolia were 16.44, 14.63, and 13.12 TWh (Figure 13b). Benefits in the main benefiting provinces did not increase in the same proportion across the two capacity levels. Changes in the national annual reduction therefore also reflected shifts in regional contributions.

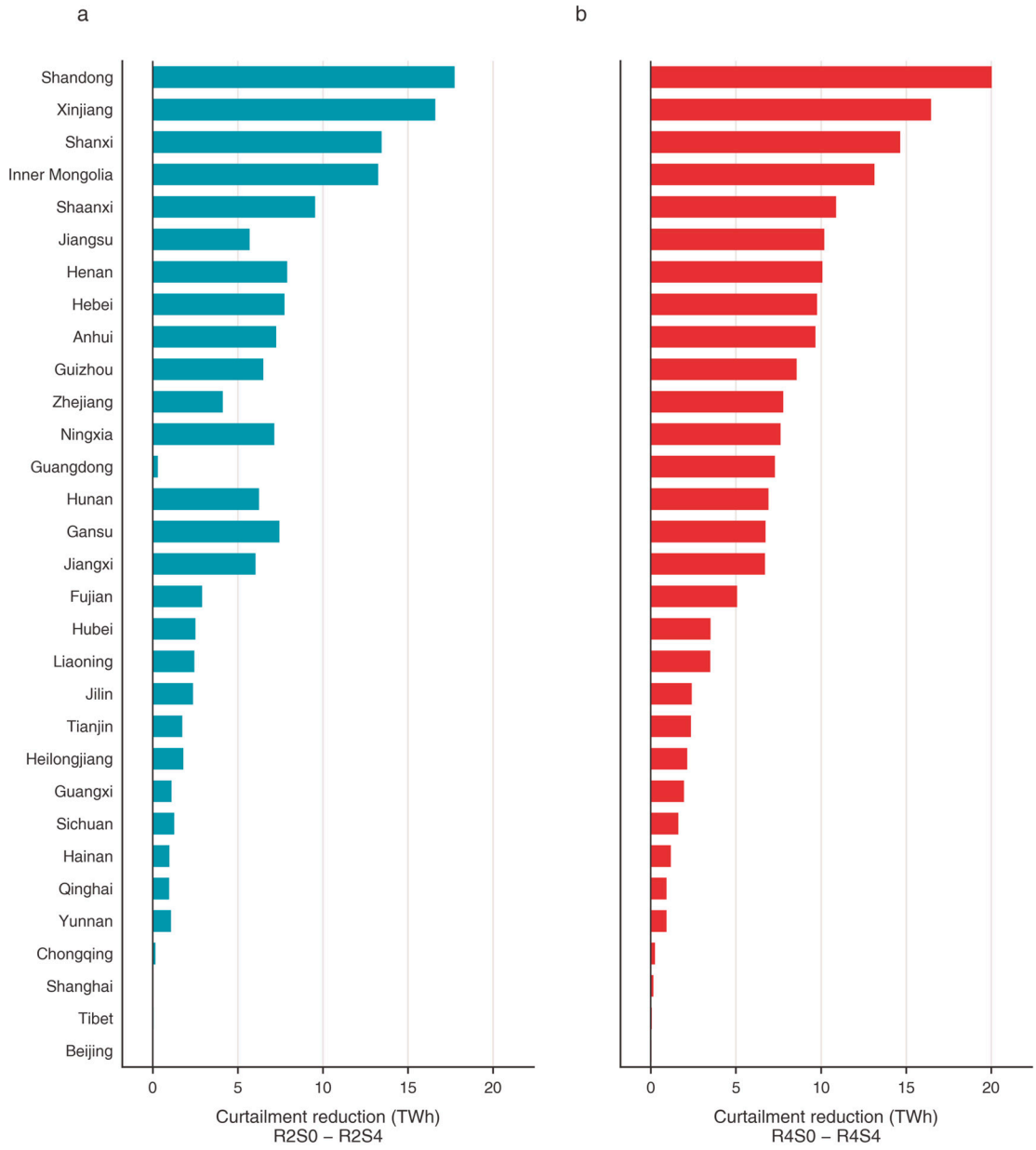


Figure 13. Provincial reductions in curtailment under the combined retrofit scenarios. (**a**) Reductions in annual curtailment in R2S4 relative to R2S0; (**b**) reductions in R4S4 relative to R4S0.

5. Discussion

5.1. Temporal Mismatch and the Limits of Renewable Capacity Expansion

The utilization benefit of renewable capacity expansion depends on the temporal and spatial alignment of additional generation with the system's capacity to accommodate it. When the capacity multiplier increased from 1.00 to 2.00, available wind and solar energy doubled. Actual generation increased by 51.4%, while the utilization rate fell from 91.4% to 69.2%. Additional curtailment was concentrated around midday. During these hours, surplus generation increased faster than the available flexibility could accommodate it. Hu et al. showed that wind–solar complementarity and regional coordination can affect the level of renewable integration [45]. The continuous hourly results presented here further indicate that utilization gains from capacity expansion are constrained by operating conditions during high-output periods. For renewable deployment, installed capacity alone does not indicate how much of the available electricity the system can actually use.

Regional variation in curtailment growth was also obscured by the national utilization rate. Inner Mongolia, Xinjiang, Hebei, Shandong, and Gansu together accounted for approximately 44% of the additional curtailment in R4 relative to R0. These regions merit particular attention when accommodation constraints are identified and flexibility resources are allocated. However, appropriate measures depend on local generation profiles, demand, and the generation mix. Spatial planning research has likewise emphasized that renewable deployment should be assessed jointly with transmission and storage provision [46]. Notably, unserved energy remained close to zero in all renewable-capacity-only scenarios. Under the conditions modelled here, capacity expansion primarily increased curtailment pressure. Renewable utilization and supply reliability therefore represented distinct dimensions of system performance.

5.2. Coupled Thermal Constraints and Asymmetric Retrofit Effects

Minimum stable output and ramp rates determine the lowest attainable thermal output and how quickly that output can be reached, respectively. Retrofit benefits therefore depend on how often each constraint binds during operation. Deep turndown alone reduced annual curtailment by approximately 25.0 TWh. By contrast, increasing bidirectional ramp rates alone reduced it by only about 0.007 TWh. The model attributed much less baseline curtailment to downward ramping than to minimum stable output. In these scenarios, the utilization gain was therefore driven mainly by a lower thermal operating limit. Research on coal-fired power retrofits has likewise distinguished the technical and cost implications of minimum-load capability, ramping performance, and retrofit scale [47].

Deep turndown also changed the thermal output adjustments required in subsequent hours. S1 reduced midday curtailment but produced approximately 45.5 GWh of unserved energy, mainly in the evening. The model attributed this shortfall to the upward-ramping constraint. After ramp-rate improvements were added in S3, a similar curtailment reduction was retained, while unserved energy approached zero. This comparison illustrates the inter-hour nature of thermal flexibility. Lower midday output created more room for renewable generation, but output had to recover as evening net load increased. Unit-level research under deep-turndown conditions has also linked low-load operation to permissible upward ramp rates [48]. Thus, deep turndown should be evaluated against both curtailment and supply balance. The value of bidirectional ramp-rate improvements is not fully captured by annual curtailment alone.

5.3. Scale-Dependent Retrofit Benefits and Coordination with Other Flexibility Resources

The combined retrofit reduced curtailment at each renewable capacity level, but its absolute and relative benefits followed different patterns. At capacity multipliers of 1.00, 1.50, and 2.00, S4 reduced curtailment by approximately 38.5, 155.5, and 191.7 TWh, respectively. The corresponding relative reductions were 14.1%, 16.6%, and 9.8%. Higher capacity levels created more surplus generation that could be accommodated by reducing thermal output. However, the amount of surplus energy remaining beyond the effect of the specified retrofit parameters also increased. Retrofit value therefore depends on both the absolute curtailment reduction and its share of total curtailment. Research on the transition of coal power from baseload generation to flexibility provision has similarly emphasized its dependence on regional generation mixes and system transition pathways [49].

After the S4 retrofit, curtailment remained at approximately 782.5 TWh in R2S4 and 1760.0 TWh in R4S4. These residual amounts warrant assessment of additional flexibility options at higher renewable capacity levels. Thermal retrofits can expand the low-output operating range of existing units and support responses to changes in net load. Storage, interregional power exchange, and demand-side flexibility may address inter-hour energy shifting, spatial imbalances, and load timing, respectively. Their incremental effects and interactions with thermal retrofits are not quantified in the present scenarios. Previous hourly analysis has compared the roles of flexible coal generation and battery storage [50]. Spatial planning research has also linked renewable deployment with transmission and storage provision [45]. For the system examined here, the incremental effects of these resources should be tested separately, with attention to curtailment hours and regions receiving the largest benefits. Operating gains and retrofit costs can then be assessed within a common allocation framework.

6. Conclusions

Under high renewable penetration, the effects of capacity expansion and thermal power flexibility retrofits depend on hourly operating conditions. Annual generation, renewable curtailment, and supply reliability do not necessarily improve together when a single parameter is changed.

Renewable capacity expansion increased actual wind and solar generation, but it also substantially increased curtailment. As the capacity multiplier rose from 1.00 to 2.00, available wind and solar generation doubled, whereas actual generation increased by 51.4%. Annual curtailment rose from 273.4 to 1951.7 TWh, and the utilization rate fell from 91.4% to 69.2%. Additional curtailment was concentrated around midday and was unevenly distributed across regions. Annual unserved energy remained close to zero in all capacity-expansion scenarios. Under the load and operating conditions examined here, further capacity expansion therefore increased the accommodation pressure during high-output hours without a discernible improvement in supply reliability.

The retrofit scenarios revealed distinct roles for minimum stable output and ramping capability. At the baseline renewable capacity level, lowering minimum stable output alone reduced curtailment by 25.0 TWh, whereas increasing upward and downward ramp rates alone reduced it by approximately 0.007 TWh. Curtailment associated with minimum stable output was much greater than that associated with downward ramping in the baseline scenario. However, improved renewable accommodation did not ensure supply balance in subsequent hours. Scenario S1 reduced midday curtailment but resulted in 45.49 GWh of unserved energy, mainly in the evening. When ramping capability was also increased in S3, a similar reduction in curtailment was retained while unserved energy fell to nearly zero. Lower minimum stable output thus expanded the accommodation space during periods of high renewable generation, whereas the principal contribution of

greater ramping capability in these scenarios was to support output recovery after low-output operation.

The effects of the combined retrofit varied with renewable capacity. At capacity multipliers of 1.00, 1.50, and 2.00, S4 reduced curtailment by 38.5, 155.5, and 191.7 TWh, respectively, relative to the corresponding no-retrofit scenarios. These reductions represented 14.1%, 16.6%, and 9.8% of baseline curtailment at each capacity level. Thus, the absolute reduction increased across the capacity levels examined, whereas the relative reduction rose and then fell. Even with S4 at a capacity multiplier of 2.00, annual curtailment remained at 1760.0 TWh. Thermal power retrofits can therefore improve renewable accommodation, but they cannot offset a fixed proportion of the additional curtailment caused by capacity expansion.

7. Implications and Future Works

7.1. Theoretical and Practical Implications

Thermal power flexibility cannot be characterized by minimum stable output or ramping capability alone. The former defines the lower operating limit during periods of low net load. The latter determines whether the required output can be reached in time and whether generation can subsequently be restored. The difference in unserved energy between S1 and S3 indicates that these constraints interact across successive hours. Evaluations of retrofit value should therefore identify when each constraint is binding and assess its distinct effects on renewable curtailment and unserved energy.

These findings inform the selection of retrofit pathways. Where curtailment is primarily associated with the minimum-stable-output constraint, lowering the operating limit can expand renewable accommodation. However, upward regulation capability must also be assessed for the evening hours. Where rapid changes in net load are the main constraint, ramping capability in the relevant direction should be prioritized. The provincial results further show that additional curtailment and retrofit benefits are concentrated in certain regions. A uniform national retrofit coverage rate may therefore obscure differences in regional benefits. Retrofit targets and coverage should be determined using local hourly net-load profiles, constraint attribution, and unserved energy. The potential contributions of storage, interregional transmission, and demand response to the curtailment remaining in high-capacity scenarios require separate scenario tests; they cannot be inferred from residual curtailment alone. Retrofit planning should therefore consider curtailment and modeled supply shortfalls together, using local hourly conditions to identify where flexibility improvements are most useful.

7.2. Limitations and Future Works

The study uses one year of load and weather data and does not capture interannual variability, extreme events, or forecast errors. Thermal operating limits are represented parametrically, without explicit unit commitment, heat–power coupling, or forced outages. Storage dispatch and interprovincial exchanges retain their PyPSA baseline schedules across scenarios. Retrofit coverage is applied uniformly to aggregate provincial capacity; the model does not identify eligible units or test alternative regional allocations. Retrofit costs and plant-level technical feasibility are also not assessed. Thus, the 80% coverage in S4 is a conditional operating scenario, not evidence that deployment at this scale is technically or economically feasible.

Future research could test the robustness of these findings using multi-year data and extreme-event scenarios. Unit-commitment modelling could provide a more detailed representation of thermal output recovery after deep turndown. Alternative storage dispatch strategies, including evening-peak state-of-charge reservation, could be compared with

the fixed baseline schedule. Unit-level technical and cost data could then be used to assess retrofit eligibility, achievable performance, and province-specific allocation. Finally, storage, interregional transmission, and demand response could be jointly optimized while accounting for retrofit investment, operating costs, fuel consumption, and carbon costs.

Supplementary Materials: The following supporting information can be downloaded at https://www.mdpi.com/article/10.3390/su182111121/s1. Table S1: Research design and flexibility dimensions of the reviewed studies; Table S2: Scenario comparisons, established findings and objectives of the present study. References [4,5,7–9,13,15,17,23–28,30,34,36,39,40,42] are cited in the Supplementary Materials.

Author Contributions: Conceptualization, R.L. and C.Z. (Changchun Zhou); methodology, R.L.; validation, R.L., C.Z. (Changchun Zhou) and X.S.; formal analysis, R.L.; investigation, C.S. and C.Z. (Cheng Zhong); resources, C.Z. (Changchun Zhou); data curation, C.S., C.Z. (Cheng Zhong) and T.F.; writing—original draft preparation, R.L.; writing—review and editing, X.S.; visualization, C.S.; funding acquisition, T.F. All authors have read and agreed to the published version of the manuscript.

Funding: This research was funded by the Science and Technology Project of Global Energy Interconnection Group Co., Ltd., under the project "Study on Quantitative Modeling of Energy and Power Policies and Evaluation of Policy Implementation Effects for Low-Carbon Transition," grant number SGGE0000JJJS2600096, and by the Fundamental Research Funds for the Central Universities (Seek-Truth Scholar), grant number 3-7-9-2024-10.

Institutional Review Board Statement: Not applicable.

Informed Consent Statement: Not applicable.

Data Availability Statement: The PyPSA and SD model code and supporting data, including processed inputs, scenario parameters, and figure source data, are available from the corresponding author upon reasonable request. The sources of external input data are cited in the manuscript.

Conflicts of Interest: Rong Li and Changchun Zhou are employed by Global Energy Interconnection Group Co., Ltd. The company's role as a funding sponsor was limited to financial support; it had no role in the study design, data collection, analysis or interpretation, manuscript preparation, or the decision to publish. The authors declare no other conflicts of interest.

References

1. National Energy Administration National Energy Administration Holds the National Renewable Energy Power Development and Construction Dispatch Video Conference (January). Available online: https://www.nea.gov.cn/20260212/7778cf9907bf4eabb0e73a939ff2ade2/c.html (accessed on 16 October 2026).
2. National Energy Administration Interpretation of the Special Action Plan for Optimizing Power System Regulation Capacity (2025–2027). Available online: https://www.nea.gov.cn/20250106/741c84c8cce04799b1561d6a45126b01/c.html (accessed on 23 October 2026).
3. International Energy Agency Market and System Operation—Introduction to System Integration of Renewables. Available online: https://www.iea.org/reports/introduction-to-system-integration-of-renewables/market-and-system-operation (accessed on 16 October 2026).
4. Ye, L.-C.; Lin, H.X.; Tukker, A. Future Scenarios of Variable Renewable Energies and Flexibility Requirements for Thermal Power Plants in China. *Energy* **2019**, *167*, 708–714. https://doi.org/10.1016/j.energy.2018.10.174.
5. Chen, X.; Wang, J.; Wang, Z.; Davidson, M.R.; MacDonald, R.; Song, J.; He, G. A Planning Model for Flexibility Retrofitting of Coal-Fired Power Plants. In *Proceedings of the 2024 3rd International Conference on Power Systems and Electrical Technology (PSET)*; IEEE: Tokyo, Japan, 2024; pp. 921–926.

6. Bu, Y.; Zhang, X. On the Way to Integrate Increasing Shares of Variable Renewables in China: Experience from Flexibility Modification and Deep Peak Regulation Ancillary Service Market Based on MILP-UC Programming. *Sustainability* **2021**, *13*, 2446. https://doi.org/10.3390/su13052446.
7. Novan, K.; Wang, Y. Estimates of the Marginal Curtailment Rates for Solar and Wind Generation. *J. Environ. Econ. Manage.* **2024**, *124*, 102930. https://doi.org/10.1016/j.jeem.2024.102930.
8. Newbery, D.M.; Biggar, D.R. Marginal Curtailment of Wind and Solar PV: Transmission Constraints, Pricing and Access Regimes for Efficient Investment. *Energy Policy* **2024**, *191*, 114206. https://doi.org/10.1016/j.enpol.2024.114206.
9. Yan, S.; Zhang, Y.; Yin, W.; Li, B.; Ye, J.; Wu, Y.; Zhang, Y. Flexibility Enhancement of Renewable-Penetrated Power Systems Coordinating Energy Storage Deployment and Deep Peak Regulation of Thermal Generators. *Electr. Power Syst. Res.* **2024**, *231*, 110354. https://doi.org/10.1016/j.epsr.2024.110354.
10. Zhao, Q.; Zhang, Y.; Zhou, X.; Chen, Z.; Yan, H.; Yang, H. A Discussion on the Flexible Regulation Capacity Requirements of China's Power System. *Engineering* **2024**, *33*, 12–16. https://doi.org/10.1016/j.eng.2023.11.015.
11. Grochowicz, A.; Benth, F.E.; Zeyringer, M. Spatio-Temporal Smoothing and Dynamics of Different Electricity Flexibility Options for Highly Renewable Energy Systems—Case Study for Norway. *Appl. Energy* **2024**, *356*, 122338. https://doi.org/10.1016/j.apenergy.2023.122338.
12. Tournier, O.; Pineau, P.-O. Maintaining Reliability in a 100% Decarbonized Power Sector: The Interrelated Role of Flexible Resources. *Energy Policy* **2024**, *195*, 114365. https://doi.org/10.1016/j.enpol.2024.114365.
13. Wei, L.; Ai, X.; Fang, J.; Lou, Y.; Liao, S.; Wen, J. Chronological Operation Simulation for Power System with Peak Regulation Ancillary Service Market in China: Formulation, Solving, and Validation. *Int. J. Electr. Power Energy Syst.* **2023**, *152*, 109156. https://doi.org/10.1016/j.ijepes.2023.109156.
14. Wang, Y.; Shen, J.; Guo, X.; Ma, X.; Ge, L.; Cheng, C. A Chronological 8760-Hour Production Simulation for Optimizing the Operation of Integrated Wind-Solar-Pumped Storage-Thermal Power Systems. *Renew. Energy* **2026**, *269*, 125863. https://doi.org/10.1016/j.renene.2026.125863.
15. Liu, H.; Andresen, G.B.; Greiner, M. Cost-Optimal Design of a Simplified Highly Renewable Chinese Electricity Network. *Energy* **2018**, *147*, 534–546. https://doi.org/10.1016/j.energy.2018.01.070.
16. Brown, T.; Hörsch, J.; Schlachtberger, D. PyPSA: Python for Power System Analysis. *J. Open Res. Softw.* **2018**, *6*, 4. https://doi.org/10.5334/jors.188.
17. Zhou, X.; Strunz, K.; Brown, T.; Sun, H.; Neumann, F. Multi-Energy System Horizon Planning: Early Decarbonisation in China Avoids Stranded Assets. *Energy Internet* **2024**, *1*, 81–98. https://doi.org/10.1049/ein2.12011.
18. Rahman, M.M.; Dadon, S.H.; He, M.; Giesselmann, M.; Hasan, M.M. An Overview of Power System Flexibility: High Renewable Energy Penetration Scenarios. *Energies* **2024**, *17*, 6393. https://doi.org/10.3390/en17246393.
19. Kondziella, H.; Bruckner, T. Flexibility Requirements of Renewable Energy Based Electricity Systems—A Review of Research Results and Methodologies. *Renew. Sustain. Energy Rev.* **2016**, *53*, 10–22. https://doi.org/10.1016/j.rser.2015.07.199.
20. Hu, S.; Yang, J.; Guo, Y.; Bi, Y.; Nan, J. Study on the Evolutionary Process and Balancing Mechanism of Net Load in Renewable Energy Power Systems. *Energies* **2024**, *17*, 4654. https://doi.org/10.3390/en17184654.
21. Rubasinghe, O.; Zhang, T.; Zhang, X.; Choi, S.S.; Chau, T.K.; Chow, Y.; Fernando, T.; Iu, H.H.-C. Highly Accurate Peak and Valley Prediction Short-Term Net Load Forecasting Approach Based on Decomposition for Power Systems with High PV Penetration. *Appl. Energy* **2023**, *333*, 120641. https://doi.org/10.1016/j.apenergy.2023.120641.
22. Sreekumar, S.; Yamujala, S.; Sharma, K.C.; Bhakar, R.; Simon, S.P.; Rana, A.S. Flexible Ramp Products: A Solution to Enhance Power System Flexibility. *Renew. Sustain. Energy Rev.* **2022**, *162*, 112429. https://doi.org/10.1016/j.rser.2022.112429.
23. Hou, Q.; Zhang, N.; Du, E.; Miao, M.; Peng, F.; Kang, C. Probabilistic Duck Curve in High PV Penetration Power System: Concept, Modeling, and Empirical Analysis in China. *Appl. Energy* **2019**, *242*, 205–215. https://doi.org/10.1016/j.apenergy.2019.03.067.
24. Yamujala, S.; Kushwaha, P.; Jain, A.; Bhakar, R.; Wu, J.; Mathur, J. A Stochastic Multi-Interval Scheduling Framework to Quantify Operational Flexibility in Low Carbon Power Systems. *Appl. Energy* **2021**, *304*, 117763. https://doi.org/10.1016/j.apenergy.2021.117763.
25. Li, B.; Feng, C.; Siebenschuh, C.; Zhang, R.; Spyrou, E.; Krishnan, V.; Hobbs, B.F.; Zhang, J. Sizing Ramping Reserve Using Probabilistic Solar Forecasts: A Data-Driven Method. *Appl. Energy* **2022**, *313*, 118812. https://doi.org/10.1016/j.apenergy.2022.118812.
26. Silva, W.N.; Rego, E.E.; Albuquerque, F.P.D.; Souza, L.G.A.D.; Lourenço, L.F.N.; Salles, M.B.C. A Data-Driven Framework to Assess Flexibility Requirements under Rising Net-Load Ramps. *Sustain. Energy Grids Netw.* **2026**, *46*, 102325. https://doi.org/10.1016/j.segan.2026.102325.

27. Cui, M.; Zhang, J.; Feng, C.; Florita, A.R.; Sun, Y.; Hodge, B.-M. Characterizing and Analyzing Ramping Events in Wind Power, Solar Power, Load, and Netload. *Renew. Energy* **2017**, *111*, 227–244. https://doi.org/10.1016/j.renene.2017.04.005.
28. Gonzalez-Salazar, M.A.; Kirsten, T.; Prchlik, L. Review of the Operational Flexibility and Emissions of Gas- and Coal-Fired Power Plants in a Future with Growing Renewables. *Renew. Sustain. Energy Rev.* **2018**, *82*, 1497–1513. https://doi.org/10.1016/j.rser.2017.05.278.
29. National Renewable Energy Laboratory (Nrel), Golden, Co (United States); Usdoe Office Of Energy Efficiency And Renewable Energy (Eere), Wind And Water Technologies Office (Ee-4W); Lew, D.; Brinkman, G.; Ibanez, E.; Florita, A.; Heaney, M.; Hodge, B.; Hummon, M.; Stark, G.; et al. *Western Wind and Solar Integration Study Phase 2*; National Renewable Energy Laboratory: Golden, CO, USA, 2013; NREL/TP-5500-55588, 1095399. https://doi.org/10.2172/1095399.
30. Frew, B.; Sergi, B.; Denholm, P.; Cole, W.; Gates, N.; Levie, D.; Margolis, R. The Curtailment Paradox in the Transition to High Solar Power Systems. *Joule* **2021**, *5*, 1143–1167. https://doi.org/10.1016/j.joule.2021.03.021.
31. National Renewable Energy Laboratory (Nrel), Golden, Co (United States); Usdoe Office Of Energy Efficiency And Renewable Energy (Eere); Strategic Analysis Team; Denholm, P.; Schwarz, M.; Streitmatter, L. *Achieving an 80% Renewable Portfolio in Alaska's Railbelt: Cost Analysis*; National Renewable Energy Laboratory: Golden, CO, USA, 2024.
32. Denholm, P.; Brinkman, G.; Mai, T. How Low Can You Go? The Importance of Quantifying Minimum Generation Levels for Renewable Integration. *Energy Policy* **2018**, *115*, 249–257. https://doi.org/10.1016/j.enpol.2018.01.023.
33. Yuan, R.; Liu, M.; Chen, W.; Yan, J. Costs versus Revenues of Flexibility Enhancement Techniques for Thermal Power Units in Electricity-Carbon Joint Markets. *Energy* **2024**, *302*, 131925. https://doi.org/10.1016/j.energy.2024.131925.
34. Fan, H.; Li, T.; Jia, Q.-S.; Zhuang, M. Multi-Timescale Synergistic Planning for Flexible Regulation of Thermal Power to Support Wind-Photovoltaic-Storage. *IET Renew. Power Gener.* **2024**, *18*, 604–615. https://doi.org/10.1049/rpg2.12925.
35. Ma, J.; Liu, Y.; Zhang, S.; Wu, L.; Yang, Z. Comprehensive Probabilistic Assessment on Capacity Adequacy and Flexibility of Generation Resources. *Int. J. Electr. Power Energy Syst.* **2023**, *145*, 108677. https://doi.org/10.1016/j.ijepes.2022.108677.
36. Jiang, J.; Zhu, Y.; Wang, Y.; Guo, X.; Lv, J.; Qin, J.; Yan, X.; Zhang, K. Unit Commitment with Bidirectional Ramping Constraints of Flexibility Retrofit Thermal Power Unit. *Int. J. Electr. Power Energy Syst.* **2025**, *168*, 110709. https://doi.org/10.1016/j.ijepes.2025.110709.
37. Li, J.; Lu, T.; Yi, X.; An, M.; Hao, R. Energy Systems Capacity Planning under High Renewable Penetration Considering Concentrating Solar Power. *Sustain. Energy Technol. Assess.* **2024**, *64*, 103671. https://doi.org/10.1016/j.seta.2024.103671.
38. Han, J.; Tan, Q.; Ding, Y.; Liu, Y. Exploring the Diffusion of Low-Carbon Power Generation and Energy Storage Technologies under Electricity Market Reform in China: An Agent-Based Modeling Framework for Power Sector. *Energy* **2024**, *308*, 133060. https://doi.org/10.1016/j.energy.2024.133060.
39. Lyu, R.; Li, A.; Wang, J.; Luo, H.; Shen, Y.; Guo, H.; Du, E.; Kang, C.; Jenkins, J. Industrial Overcapacity Can Enable Seasonal Flexibility in Electricity Use. *Nat. Energy* **2026**, *11*, 1203–1215. https://doi.org/10.1038/s41560-026-02073-y.
40. Martínez-Jaramillo, J.E.; Van Ackere, A.; Larsen, E.R. Transitioning towards a 100% Solar-Hydro Based Generation: A System Dynamic Approach. *Energy* **2022**, *239*, 122360. https://doi.org/10.1016/j.energy.2021.122360.
41. Pourramezan, A.; Samadi, M. A System Dynamics Investigation on the Long-Term Impacts of Demand Response in Generation Investment Planning Incorporating Renewables. *Renew. Sustain. Energy Rev.* **2023**, *171*, 113003. https://doi.org/10.1016/j.rser.2022.113003.
42. Luo, Y.; Ahmadi, E.; McLellan, B.C.; Tezuka, T. A Hybrid System Dynamics Model for Power Mix Trajectory Simulation in Liberalized Electricity Markets Considering Carbon and Capacity Policy. *Renew. Energy* **2024**, *233*, 121164. https://doi.org/10.1016/j.renene.2024.121164.
43. National Energy Administration Grid-Connected Operation of Renewable Energy in 2025. Available online: https://www.nea.gov.cn/20260212/742b8c6a078347b0b39de676c05c5d58/c.html (accessed on 23 October 2026).
44. Levin, T.; Bistline, J.; Sioshansi, R.; Cole, W.J.; Kwon, J.; Burger, S.P.; Crabtree, G.W.; Jenkins, J.D.; O'Neil, R.; Korpås, M.; et al. Energy Storage Solutions to Decarbonize Electricity through Enhanced Capacity Expansion Modelling. *Nat. Energy* **2023**, *8*, 1199–1208. https://doi.org/10.1038/s41560-023-01340-6.
45. Hu, Y.; Jiang, H.; Zhang, C.; Yuan, J.; Zhang, M.; Yao, L.; Chen, Q.; Wu, J.; Zhang, H.; Ma, S.; et al. Advancing Solar and Wind Penetration in China through Energy Complementarity. *Nature* **2026**, *653*, 1060–1068. https://doi.org/10.1038/s41586-026-10570-z.
46. Zhu, Z.; Ma, S.; Mao, H.; Zhong, J.; Guo, L.; Wang, D.; Huang, J.; Miao, C.; Zhang, X.; Zhang, X.; et al. Spatial Planning for China's Renewable Energy Expansion toward 2030. *Appl. Energy* **2025**, *398*, 126413. https://doi.org/10.1016/j.apenergy.2025.126413.

47. Ping, L.; Wang, P.; Guo, Y.; Lin, Y.; Wang, Y.; Tong, D. Optimizing Flexibility Retrofits of China's Coal Fleet in a Renewables-Dominant Future. *Energy* **2026**, *360*, 141702. https://doi.org/10.1016/j.energy.2026.141702.
48. Liu, Z.; Wang, C.; Fan, M.; Wang, Z.; Fang, F.; Liu, M.; Yan, J. Investigation on the Allowable Load Ramping-up Rate and Wet-to-Dry Conversion Time of a 660 MW Supercritical Coal-Fired Power Plant with Deep Peak-Shaving Work Conditions. *Energy* **2025**, *314*, 134200. https://doi.org/10.1016/j.energy.2024.134200.
49. An, K.; Zheng, X.; Shen, J.; Xie, C.; Wang, C.; Cai, W.; Bu, C. Repositioning Coal Power to Accelerate Net-Zero Transition of China's Power System. *Nat. Commun.* **2025**, *16*, 2311. https://doi.org/10.1038/s41467-025-57559-2.
50. Lin, B.; Liu, Z. Assessment of Flexible Coal Power and Battery Energy Storage System in Supporting Renewable Energy. *Energy* **2024**, *313*, 133805. https://doi.org/10.1016/j.energy.2024.133805.

Disclaimer/Publisher's Note: The statements, opinions and data contained in all publications are solely those of the individual author(s) and contributor(s) and not of MDPI and/or the editor(s). MDPI and/or the editor(s) disclaim responsibility for any injury to people or property resulting from any ideas, methods, instructions or products referred to in the content.